Monte Carlo Calculation of the Penetration and Diffusion of Fast Charged Particles*

MARTIN J. BERGER

NATIONAL BUREAU OF STANDARDS
WASHINGTON, D.C.

I. Introduction

THIS ARTICLE IS CONCERNED with the simulation, by random sampling, of the multiple Coulomb scattering of fast charged particles, for the purpose of solving electron and proton transport problems. Direct simulation of the physical scattering processes would be laborious because of the large number of Coulomb interactions that occur even in a short pathlength. An alternative approach is used instead, in which the diffusion process is imitated by letting the particles carry out an

* Work supported by the Office of Naval Research.

(artificially constructed) random walk, each step of which takes into account the combined effect of many collisions.

The state of the art of solving transport problems for fast charged particles can be indicated as follows. The mathematical complexities are considerable, because of the large number of variables (up to six) that enter into the transport equation, and because of the variety of interactions that may have to be considered jointly: elastic scattering by atomic nuclei, inelastic scattering by atomic electrons, production of secondary knock-on electrons, bremsstrahlung, and—possibly—nuclear interactions. When traversing even a thin layer of matter, an electron or proton will make an enormous number of collisions that result in small energy losses and deflections, and a relatively small number of "catastrophic" collisions in which they may lose a major fraction of their energy or may be turned through a large angle. The combined effect of all collisions is a complex process of diffusion and energy degradation whose realistic description requires an elaborate theory.

Ever since the end of the nineteenth century, when fast charged particles first became available to the experimenter, multiple scattering has received the attention of many prominent theorists, and a flourishing subbranch of mathematical physics has developed around the solution of the transport equation. The early phases of this work have been surveyed by Bothe (1933), and later work has been summarized by Rossi (1952), Fano (1953), and Birkhoff (1958), among others. The available multiple-scattering theories provide accurate predictions and have been well confirmed by experiments. Yet their applicability is limited because of the more or less severe restrictions that were necessary for an analytical treatment to be possible. For example, the theories of Williams (1939), Snyder and Scott (1949), and Molière (1948) describe angular distributions only, make the small-angle approximation, and consider energy loss either not at all or only with the disregard of statistical fluctuations. On the other hand, the theories of Landau (1944) and of Blunck and Leisegang (1950) deal with fluctuations in energy loss only, and assume the loss to be small compared with the initial energy of the multiply-scattered particle. The theory of Goudsmit and Saunderson (1940) places no limitation on the magnitude of the angular deflections, but disregards spatial deflections resulting from multiple scattering, a limitation that is shared by all the theories mentioned before. The moment-method of Lewis (1950) and Spencer (1955, 1959) is more complete in that it takes into account the spatial and angular aspects of the diffusion phenomenon, and has been extended to include fluctuations in energy loss (Spencer, private communication), but it is

limited to applications where the medium is unbounded and homogeneous. This restriction also holds for the other theories mentioned above. Treatments assuming more realistic boundary conditions have been given by Fermi (see Rossi, 1952) who used a small-angle approximation, and by Bethe *et al.* (1938) whose work in turn was extended by Weymouth (1951), Roesch (1954), Meister (1958), and Archard (1961). This work is based on a simplified version of the transport equation (diffusion approximation) and is therefore restricted in its applicability. Finally, formal treatments such as those of Wentzel (1922), Wang and Guth (1951), and Breitenberger (1959) in principle yield general solutions, but in practice can be evaluated only with the use of drastic simplifications so that their generality is lost.

There is a large class of problems that arise in the context of experimental, technical or radiological physics for which presently available multiple scattering theories do not provide adequate answers. To mention a few typical examples: an experimenter may want to know the effect of the backscattering of electrons from components of a beta-ray spectrometer; he may be interested in the probability that an electron resulting from the decay of a stopped meson can reach a detector in a given experimental configuration; he may want to know how multiple scattering affects the response of radiation detectors such as ionization chambers, scintillation counters, and photographic plates. Beams of charged particles are often passed through thick layers of material to bring their energy to a desired value, and one would like to know the fluctuations in energy of the emerging particle beam. The radiological physicist may be interested in the transfer of energy from an X-ray or bremsstrahlung beam to secondary electrons which in turn distribute it to the medium. In all these problems, the boundary conditions imposed by the experimental configuration tend to be complicated, statistical fluctuations of energy losses and deflections may be of importance, and large losses and deflections cannot be disregarded.

Modern computers are a powerful new tool for the solution of such problems. There is a temptation to jettison analytical methods altogether, and to rely entirely on numerical methods. This could be done either by numerical integration of the transport equation, or by random sampling. The former approach, which—to the author's knowledge—has not yet been attempted, would be a formidable undertaking, in part because of the large number of the variables in the transport equation. However, a calculation patterned, for example, after the S_n method developed by Carlson (1955) for neutrons might very well be feasible. Random sampling by a direct analog Monte Carlo procedure would be quite costly, because of the enormous number of collisions

that must be sampled. It should be mentioned, however, that MacCallum (1960) has reported a calculation of electron backscattering by this method.

In the present article we shall employ an approach in which numerical computation does not have an exclusive role but serves to combine several multiple-scattering theories into a coherent scheme. Each of the component theories covers some aspect of the diffusion phenomenon with particular accuracy, and the combination of theories is characterized by increased flexibility and applicability. Such an approach for charged particles was first used by Hebbard and Wilson (1955) and later by Sidei *et al.* (1957), Leiss *et al.* (1957), and Berger (1960). The essential feature is the grouping of many steps of the actual physical random walk into a single step of a "condensed" random walk. The transition probabilities for the condensed random walk are given by the appropriate multiple-scattering theories, and the number of steps in a walk are kept small enough (not more than, say, 100) so that a large number of walks can be sampled in a reasonable amount of time. Once the necessary grouping has been decided upon, the remaining Monte Carlo problem is similar to those encountered in conventional random-sampling treatments of neutron or gamma-ray transport problems. Thus the computations are relatively easy to set up, even if the boundary conditions and configuration of the medium are complex, but they are time-consuming and require a vast amount of predigested information to be stored in the computer memory. One could almost say that the problem is one of data processing rather than of analysis.

The multiple-scattering theories introduced into the Monte Carlo scheme are not quite complete. This, together with the effects of grouping, introduces some arbitrariness, and leads to a systematic error which is superimposed on the statistical error associated with random sampling. One of the purposes of the present work is to present a fairly substantial body of results by means of which this systematic error can be estimated by internal evidence and through comparison with experiments of independent calculations. For this reason, problems have been chosen which are typical but simple, involving one space variable only. Thus many of the comparisons will have to do with the reflection from, transmission through, and energy dissipation in thick foils. Relatively little will be said about bremsstrahlung, and even less about nuclear interactions, because of the scarcity of relevant calculational experience.

The computations to be described, insofar as carried out by the author, were accomplished with an IBM 704 computer. They are discussed from the standpoint of a physicist who does his own programming in a simplified coding language (FORTRAN), and who is

intent on minimizing not only the machine running time but also the coding effort. Thus little attention is given to ways in which the computations could be speeded up through refined programming techniques in basic machine language, and efficiency is sought primarily through a suitable layout of the flow of calculation.

II. General Description of the Monte Carlo Method

A. Relation to Transport Equation

Although no direct use will be made of the transport equation in the sequel, we shall write it down briefly, in order to indicate the mathematical problems to be solved implicitly by the Monte Carlo method. It is a linear integro-differential equation of the form

$$\frac{1}{v}\frac{\partial F}{\partial t} + \mathbf{u}\cdot\nabla F + \mu F = \int_E^\infty dE' \int_{4\pi} d\mathbf{u}' F(E', \mathbf{u}', \mathbf{r}, t)\,\psi(E', \mathbf{u}', E, \mathbf{u})\,, \quad (1)$$

where

t = time

v = particle velocity

$F(E, \mathbf{u}, \mathbf{r}, t)\,dE\,d\mathbf{u}$ = flux of particles, at time t and position $\mathbf{r}$, with energies in the interval $(E, E + dE)$ and directions in the interval $(\mathbf{u}, \mathbf{u} + d\mathbf{u})$. (Flux is defined as the number of particles that cross per unit time through a unit area of a surface perpendicular to $\mathbf{u}$.)

$\mu(E)$ = probability, per unit pathlength, of an interaction of any type between the particle and the medium.

$\psi(E', \mathbf{u}'; E, \mathbf{u})\,dE\,d\mathbf{u}$ = probability, per unit pathlength, that a particle with energy E' and direction $\mathbf{u}'$ will, as the result of a collision, acquire an energy in the interval $(E, E + dE)$ and a direction in the interval $(\mathbf{u}, \mathbf{u} + d\mathbf{u})$. If the flux of secondary electrons is also of interest, ψ must take into account their production, and must then be interpreted as a production rate.

The pathlength traveled by the particle may be used as a "clock" to measure time; i.e., the variable t may be replaced by the pathlength

$$s = \int_0^t v(t')\,dt'\,, \quad (2)$$

in which case the term $1/v\ \partial F/\partial t$ in the transport equation is replaced by $\partial F/\partial s$. In stationary problems, $\partial F/\partial s = 0$, so that the pathlength

variable could be dropped. In Monte Carlo calculations we shall retain it nevertheless, because it provides a useful parameter for the grouping of collisions.

Anticipating later developments, we also note that s is often allowed to play the role of an energy parameter, in the so-called *continuous slowing-down approximation*. In this approximation, fluctuations of the energy loss are disregarded, and the energy of the particle is taken to be a deterministic function of the pathlength traveled:

$$E(s) = E_0 - \int_0^s \left| \frac{dE}{ds}(s') \right| ds' , \tag{3}$$

where dE/ds is the mean energy loss per unit pathlength (stopping power).

Various assumptions enter into the derivation of the transport equation which we also take over for the Monte Carlo calculations:

(1) The scattering centers (atoms and electrons) are distributed at random, although not necessarily with uniform density; correlations between the positions of different atoms and electrons are not taken into account;

(2) The charged particle, in the course of traversing the medium, interacts with one scattering center at a time. This implies the neglect of quantum-mechanical interference (electron diffraction) resulting from the coherent scattering by several centers. The trajectory of the particle is thus idealized as a zig-zag path, consisting of free flights interrupted by sudden collisions in which the energy and direction of the particle is changed.

A description of the diffusion process in terms of the transport equation is analogous to the use of Eulerian coordinates in hydrodynamics, in that one asks about the flux at a given point in space. By contrast, the Monte Carlo method uses Lagrangian coordinates; one attaches a label to a particular bit of fluid, i.e., a diffusing particle, and follows its history.

B. Detailed Case Histories

The trajectory of a particle can be described by the array

$$E_0, E_1, E_2, \ldots, E_n, \ldots$$
$$\mathbf{u}_0, \mathbf{u}_1, \mathbf{u}_2, \ldots, \mathbf{u}_n, \ldots$$
$$\mathbf{r}_0, \mathbf{r}_1, \mathbf{r}_2, \ldots, \mathbf{r}_n, \ldots ,$$

where E_n is the energy, $\mathbf{u}_n$ the direction, and $\mathbf{r}_n$ the position immediately after the nth collision, and where the index zero refers to the initial

state of the particle. Such a trajectory can be generated by random sampling. The probability distribution for transitions from one state to the next, i.e., from one column of the array to the next, is determined by the single-scattering probabilities ψ and μ. In case the particle makes inelastic collisions in which secondary electrons are set in motion, the history of the latter must be followed separately.

By sampling many histories, one is able—in principle—to solve any diffusion problem. Suppose, for example, that we want to calculate the reflection and transmission of electrons by a foil, which is assumed to be bounded by the planes $z = 0$ and $z = d$. (See Fig. 1.) The Monte

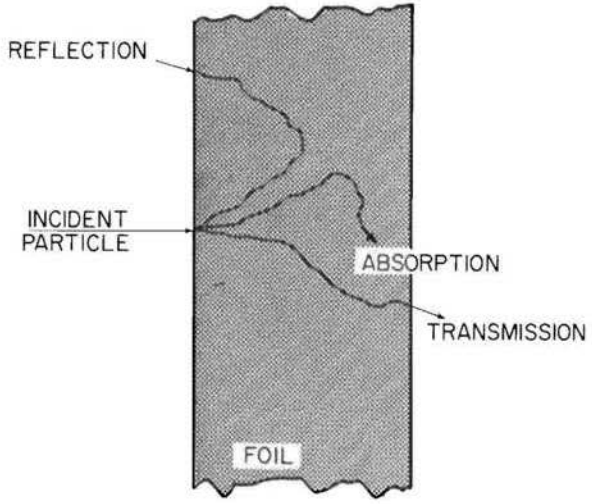

FIG. 1. Typical particle trajectories in foil.

Carlo procedure would consist of sampling many electron trajectories (usually called case histories), starting each one at $z = 0$ and following it until any one of three events happens for the first time: (1) z becomes negative (reflection), (2) z becomes greater than d (transmission), or (3) the residual range of the electron becomes so small that it can no longer escape from the foil (absorption). Dividing the scores thus obtained by the number of histories sampled, one obtains the reflection, transmission, and absorption coefficients for the foil. In order to determine these coefficients by using the transport equation, one would have to determine the reflected and transmitted currents,

$$J(z) = \int_0^{E_0} dE \int_{4\pi} d\mathbf{u} \mid \cos\theta \mid F\,, \tag{4}$$

at $z = 0$ and $z = d$ (θ is the angle between $\mathbf{u}$ and the z-axis). The flux F would have to satisfy the boundary conditions that at the exit boundary ($z = d$) no electrons travel toward smaller z, and that at the entrance boundary ($z = 0$) no electrons travel toward larger z except those in the incident beam. The exact analytical solution of this boundary problem is not known.

Because of the strength and long range of the Coulomb interaction, the number of collisions in a typical charged-particle history is enormous. Some order-of-magnitude estimates for electrons are given in Table I.

TABLE I

ESTIMATED NUMBER OF COLLISIONS MADE BY ELECTRONS IN THE COURSE OF SLOWING DOWN.[a]

Energy interval (Mev)	Aluminum	Gold
0.5 – 0.25	2.9×10^4	1.7×10^5
0.25 – 0.125	3.4×10^4	1.7×10^5
0.125 – 0.0625	4.2×10^4	1.5×10^5

[a] Based on the Rutherford scattering cross section with screening correction.

They were obtained with an assumed Rutherford scattering cross section, modified to take into account screening of the nuclear charge by orbital electrons (see Appendix, B, 2). It can be seen that for path-lengths such that the electrons lose an appreciable fraction of their energy, the average number of collisions may be in the ten- or even hundredthousands. This is in great contrast to the behavior of gamma rays or neutrons. Only 20 to 30 Compton scatterings will reduce the energy of a photon from several Mev down to 50 kev. Similarly, 18 elastic collisions in hydrogen will reduce the energy of a neutron from 2 Mev to thermal energy, and even for heavy nuclei of atomic weight A approximately $9A + 6$ collisions are sufficient for the same energy reduction. Thus electron Monte Carlo histories might be up to several hundred times longer than neutron or gamma-ray histories. It is hard to see how biased sampling or importance sampling could remove this handicap. These techniques are designed to increase the likelihood, in the Monte Carlo calculation, of events which in the physical process are quite rare. They are not designed to increase the efficiency of Monte Carlo calculations in situations where the event of interest takes place only after a very long chain of intermediate collisions.

C. Condensed Case Histories

In order to reduce the required amount of computation we abandon the complete description of charged-particle histories and limit ourselves to snapshots taken at various times during the particle's history. A sequence of such snapshots provides a "moving picture" of the history which can be used for the solution of various diffusion problems. In order to select the times at which the snapshots are taken it is convenient, although not absolutely necessary, to use as clock the pathlength traveled by the particle. Thus we introduce condensed histories

$$0,\ s_1,\ s_2,\ \ldots,\ s_n,\ \ldots$$
$$E_0, E_1, E_2, \ldots, E_n, \ldots$$
$$\mathbf{u}_0,\ \mathbf{u}_1,\ \mathbf{u}_2,\ \ldots,\ \mathbf{u}_n,\ \ldots$$
$$\mathbf{r}_0,\ \mathbf{r}_1,\ \mathbf{r}_2,\ \ldots,\ \mathbf{r}_n,\ \ldots,$$

where E_n is the energy, $\mathbf{u}_n$ the direction, and $\mathbf{r}_n$ the position of the particle when it has traveled a pathlength s_n from its starting point. A condensed history is sampled by letting the particle carry out a random walk in which each step, from state n to state $n+1$, takes into account the combined effect of many collisions. The transition probabilities for each step are determined by the appropriate multiple-scattering theories. There would be no question as to how this random walk should be set up, if a complete theory were available; but then the Monte Carlo calculation itself would become unnecessary. The important point is that even incomplete and partial theories, when suitably combined, can yield enough information so that condensed histories can be sampled with fair accuracy.

The size of the steps of the random walk, i.e., the pathlength intervals $\Delta s_n = s_{n+1} - s_n$, must be chosen with some care. On the one hand, the total *number of steps* should be kept as small as possible, because the length of the Monte Carlo calculation will be directly proportional to it. On the other hand, a small *step size* has the following advantages:

(1) In applications to boundary problems such as reflection and transmission by foils, most of the steps of the condensed history will lie entirely in the interior of the medium, so that multiple-scattering theories for unbounded media can be applied to them. Boundary affects need only be considered in the one section of the history in which the particle makes its escape from the medium. In this one step its state will not change much, so that even a very crude approximation may be adequate.

(2) The net angular deflection and energy loss in one step of the random walk are small, so that multiple-scattering theories with this restriction become applicable.

(3) Even though the correlation between deflections and energy losses within each step is disregarded by the multiple-scattering theory, this correlation is taken into account at least partially when the steps of the condensed random walk are combined.

III. Particular Monte Carlo Schemes

A scheme must provide, for each step of the random walk, a rule for selecting a pathlength $s_{n+1} - s_n$, an energy loss $E_n - E_{n+1}$, a change of direction from $\mathbf{u}_n$ to $\mathbf{u}_{n+1}$, and a spatial displacement $\mathbf{r}_{n+1} - \mathbf{r}_n$. A great variety of schemes are possible, which differ in regard to the theoretical input and the necessary amount of computation for random sampling. We shall list in this chapter some of these schemes, with emphasis on those which have actually been used. The execution of any one of these schemes takes a substantial amount of programming and computing effort, so that the list is neither as exhaustive nor as systematic as would be desirable. The multiple-scattering theories for each scheme are briefly indicated, but the detailed equations are relegated to the Appendix.

The schemes we shall discuss fall into two major categories. Class I, which is the simpler of the two, relies entirely on the grouping of collisions, and involves the use of a predetermined set of pathlengths. A variant, Class I′, is based on a predetermined set of energy losses. Class II is based on a mixed procedure in which collisions with small energy losses and deflections are subject to grouping, but occasional "catastrophic" collisions, in which the loss or deflection are very large, are treated separately by conventional random sampling according to the single-scattering cross sections.

A. Complete Grouping, Class I

1. *Pathlength*

a. Logarithmic spacing. The pathlength is chosen such that, on the average, the energy of the particle is reduced by a constant factor k per step. Given E_n and s_n, s_{n+1} is then determined from the equation

$$1 - \frac{1}{E_n} \int_{s_n}^{s_{n+1}} \left| \frac{dE}{ds} \right| ds = k , \tag{5}$$

where dE/ds is the mean rate of energy loss per unit pathlength resulting from ionization [see Eqs. (A9-12) of the appendix].

Logarithmic spacing has the advantage that the average angular multiple-scattering deflection per step changes little from step to step. This can be shown by an approximate formula derived by Blanchard and Fano (1951) and Blanchard (1951) which holds at energies where bremsstrahlung losses can be disregarded. They find that the mean value of the cosine of the deflection angle, $\langle \cos \omega \rangle_{\text{av}}$, can be estimated by the following rule of thumb:

$$\langle \cos \omega \rangle_{\text{av}} \sim \left(\frac{E_{n+1}}{E_n} \frac{E_n + 2mc^2}{E_{n+1} + 2mc^2} \right)^{0.3Z}, \tag{6}$$

where Z is the atomic number of the medium and mc^2 the rest energy of the particle. When the kinetic energies E_n and E_{n+1} are smaller than $2\,mc^2$, the angular deflection depends only on E_{n+1}/E_n, but not on E_n and E_{n+1}, separately. Therefore, logarithmic spacing has the advantage that the distribution of angular deflections changes very slowly from step-to-step. It is often convenient to set the reduction factor $k = 2^{-1/m}$, where m is an integer, so that in the absence of energy loss fluctuations the particle would lose half its energy in m steps. Table II lists characteristic data for electrons in aluminum, for $m = 16$, $k = 0.9576$, which is a typical spacing that has been found advantageous. Results presented in Section V will indicate the effect of varying the magnitude of m.

TABLE II

CHARACTERISTICS OF CONDENSED ELECTRON HISTORY IN ALUMINUM, MODEL I.

Step	Energy interval (Mev)	Δs (gm/cm²)	$\omega_{\max}$[a] (degrees)	$\langle \cos \omega \rangle_{\text{av}}$[b]
1	2.0 – 1.9152	0.057476	11.4	0.945
17	1.0 – 0.9576	0.028748	13.5	0.919
33	0.5 – 0.4788	0.013163	15.2	0.893
49	0.25 – 0.2394	0.005291	16.3	0.872
65	0.125 – 0.1197	0.001749	16.5	0.857
81	0.0625 – 0.0599	0.000603	15.8	0.848
97	0.03125 – 0.0299	0.000184	14.7	0.842

[a] $\omega_{\max}$ = angle at which $A_{GS}(\omega) \sin \omega$ peaks.

[b] $\langle \cos \omega \rangle_{\text{av}}$ and $\omega_{\max}$ computed from Goudsmit-Saunderson theory, with Mott cross section.

b. Mixed logarithmic spacing. This is a procedure that has to be adapted to the diffusion problem under consideration. When the

particle is in the interior of the medium, the logarithmic spacing described above is used with a fixed value of k (or m). But whenever the particle, in the course of its history, reaches a position such that the next step could carry it across a boundary of interest, that step is broken up into j steps with reduction factor $k' = k^{1/j}$ (or $m' = jm$). The energy and direction of the particle are well known only at the beginning and end of a step of a condensed random walk; their values at the time of the crossing of the boundary must be guessed by suitable interpolation. The error incurred thereby is reduced by forcing the crossing to occur in a very small step.

c. Uniform spacing. The step size $s_{n+1} - s_n =$ constant. With this arrangement the angular deflection increases from step-to-step. The spacing constant may eventually have to be reduced toward the end of a long history, in order to limit the angular deflections to the desired small value.

2. *Energy Loss*

a. Continuous-slowing-down approximation. The energy loss is determined from the equation

$$\Delta E_n = E_n - E_{n+1} = \int_{s_n}^{s_{n+1}} \left| \frac{dE}{ds} \right| ds \,. \tag{7}$$

If logarithmic pathlength intervals are used, $E_{n+1} = kE_n$.

b. Fluctuations of ionization loss. E_n is selected from a distribution $W_I(\Delta E)$, which has been given by Landau (1944) and further refined by Blunck and Leisegang (1950) [see Eqs. (A17-21) of the appendix]. This distribution has been derived on the assumption that $\Delta E_n \ll E_n$.

c. Fluctuation of ionization and bremsstrahlung loss. For electrons and positrons, at energies above one Mev in High-Z materials and several Mev in low-Z materials, radiative losses begin to make a significant contribution to the total energy loss. One must therefore select ΔE_n from a distribution taking both modes of energy loss into account. One such distribution has been derived by Blunck and Westphal (1951), on the assumption that $\Delta E_n \ll E_n$. They expressed it as a convolution of the ionization loss distribution $W_I(\Delta E)$ with a bremsstrahlung loss distribution $W_B(\Delta E)$,

$$W_{IB}(\Delta E_n) = \int_0^{\Delta E_n} W_I(\Delta E_n - \eta)\, W_B(\eta)\, d\eta \,. \tag{8}$$

Bremsstrahlung cross sections are complicated, and have been derived

in a great variety of approximations applicable under different conditions (see Koch and Motz, 1959); the best formulation for Monte Carlo calculations needs further investigation.

3. *Angular Deflection*

Let $\mathbf{u}_n = (\theta_n, \varphi_n)$ and $\mathbf{u}_{n+1} = (\theta_{n+1}, \varphi_{n+1})$ denote the directions of the particle at the beginning and at the end of a step, and ω and $\Delta\varphi$ the polar and azimuthal multiple-scattering deflections in that step. It is understood that θ and φ are spherical coordinates in a system with the z-axis as polar axis, whereas ω and $\Delta\varphi$ are defined with respect to a spherical-coordinate system whose polar axis coincides with the direction of motion at the beginning of the step. We have then the well-known kinematic relations between change of direction and multiple-scattering deflections.

$$\cos\theta_{n+1} = \cos\theta_n \cos\omega + \sin\theta_n \sin\omega \cos\Delta\varphi\,, \tag{9}$$

$$\sin(\varphi_{n+1} - \varphi_n) = \frac{\sin\omega \sin\Delta\varphi}{\sin\theta_{n+1}}\,, \tag{10}$$

$$\cos(\varphi_{n+1} - \varphi_n) = \frac{\cos\omega - \cos\theta_n \cos\theta_{n+1}}{\sin\theta_n \sin\theta_{n+1}}\,. \tag{11}$$

The azimuthal deflection $\Delta\varphi$ is distributed uniformly between 0 and 2π, provided the medium is isotropic and polarization is disregarded. The deflection angle ω must be selected from one of many available multiple-scattering distributions. All existing theories allow the energy loss of the particle to be taken into account in the continuous-slowing-down approximation, but disregard the effect of fluctuations of energy loss.

a. Gaussian approximation. If the net angular multiple-scattering deflection is the result of the combined effect of many small individual deflections, each of the same order of magnitude, purely statistical considerations lead to a Gaussian distribution,

$$A_G(\omega)\,\omega\,d\omega = 2(\omega/\bar{\omega}^2)\exp(-\omega^2/\bar{\omega}^2)\,d\omega\,, \tag{12}$$

which is normalized to unity in the interval $(0, \infty)$. The mean square deflection $\bar{\omega}^2$ must be calculated from the appropriate single-scattering cross section, such as the Rutherford scattering law; there are ambiguities in this procedure because large individual deflections are not allowed to contribute to $\bar{\omega}^2$ as long as one wants to preserve the validity of the Gaussian approximation. Various prescriptions for the evaluation

of ϖ^2 have been proposed (see Rossi, 1952). We shall not follow this up, because little use will be made of the Gaussian distribution in spite of its simplicity.

b. Distribution of Molière (1948). This theory takes into account the effect of occasional large individual deflection, neglected in the Gaussian approximation. It is formulated in terms of a "reduced scattering angle"

$$\vartheta = \omega/\chi_c \sqrt{B}, \tag{13}$$

where χ_c and B are parameters which express the dependence on pathlength and energy [see Eqs. (A22-28) of the appendix]. The distribution has the form

$$A_M(\omega)\, \omega\, d\omega = \vartheta\, d\vartheta \left\{ 2 \exp(-\vartheta^2) + \frac{f^{(1)}(\vartheta)}{B} + \frac{f^{(2)}(\vartheta)}{B^2} + \ldots \right\} \tag{14}$$

where $f^{(1)}$ and $f^{(2)}$ are purely numerical functions tabulated by Molière (1948) and Bethe (1953).

The applicability of the Molière theory is subject to a number of limitations:

(1) It assumes a pathlength long enough for the occurrence of at least 20 collisions on the average; for our purposes, this restriction is not important.

(2) The net multiple-scattering deflection must be small (not greater than $\sim$30 to 40 degrees).

(3) The parameters χ_c and B are evaluated on the basis of a single-scattering theory developed by Molière (1947) which is fairly exact, but does not distinguish between the scattering of positrons and electrons.

According to Bethe (1953), restriction (2) can be largely removed, and the applicability extended to large angles, through multiplication of the Molière distribution by a factor $\sqrt{\sin \omega/\omega}$. This is verified, in Table III, through a comparison—in a typical case—with a more exact theory. Restriction (3) has recently been removed by the work of Nigam *et al.* (1959) who fed into the Molière multiple-scattering formalism a single-scattering cross section based on a screened Coulomb potential and evaluated in the second Born approximation. Their theoretical distribution predicts differences in the multiple scattering of positrons and electrons (Nigam and Mathur, 1961). It has a structure similar to that of Molière, but with considerably more complicated numerical coefficients, not all of which have yet been evaluated (see also Fleischmann, 1960).

TABLE III

COMPARISON OF MOLIÈRE AND GOUDSMIT-SAUNDERSON ANGULAR MULTIPLE-SCATTERING DISTRIBUTIONS.[a]

Interval (Degrees)	Molière[b]	Goudsmit-Saunderson		
		Rutherford	Mott electrons	Mott positrons
0–15	41473	40790	40736	41405
15–30	42333	42268	42601	42796
30–45	11770	12128	12321	11936
30–45	2766	2885	2854	2600
60–75	867	961	871	751
75–90	377	432	341	284
90–120	294	368	221	182
120–150	94	133	48	40
150–180	26	35	7	6

[a] Angular distribution of electrons and positrons slowing down in aluminum from 1.0 Mev to 0.9576 Mev. Pathlength is 0.0287 gm/cm² for electrons, 0.0294 gm/cm² for positrons. Distributions are normalized to 100,000 particles.

[b] Obtained from the Molière theory with the Bethe correction for large angles, $\sqrt{\sin \omega/\omega}\, A_M(\omega)$. Applies to electrons and positrons.

c. Theory of Goudsmit and Saunderson (1940). These authors derived the exact angular distribution of multiple-scattering deflections as a Legendre series,

$$A_{GS}(\omega) \sin \omega \, d\omega = \sum_{l=0}^{\infty} \left(l + \frac{1}{2}\right) \exp\left\{-\int_0^s G_l(s')\, ds'\right\} P_l(\cos \omega) \sin \omega \, d\omega \,, \quad (15)$$

where

$$G_l(s) = 2\pi N \int_0^{\pi} \sigma(\theta, s) \{1 - P_l(\cos \theta\} \sin \theta \, d\theta \,. \quad (16)$$

N is the number of atoms per unit volume, s is the pathlength traversed by the particle, and $\sigma(\theta, s)$ is the single-scattering cross section, whose dependence on the energy is expressed, in the continuous-slowing-down approximation, through the dependence on the pathlength s.

The Goudsmit-Saunderson series has two great advantages. It applies to all angular deflections without restriction as to their magnitude, and it can be evaluated for any desired single-scattering cross section. For electrons and positrons we shall use it in conjunction with the Mott

scattering cross section, modified to take into account the screening of the nuclear charge by the orbital electrons. This cross section, which includes relativistic and spin effects, differs considerably from the Rutherford cross section at large angles, and also predicts differences in the deflection of positrons and electrons.

In Monte Carlo applications, the pathlength s is usually small enough so that $A_{GS}(\omega) \sin \omega$ peaks at small values of ω which typically range from 10° to 25° and may be even smaller if very short steps are taken near a boundary of interest. The Legendre series then converges slowly, and twenty, forty, or even a larger number of terms may have to be included. This would be a difficult and tedious task, even with a high-speed computer, if Spencer (1955, 1959) had not indicated convenient recursion relations by means of which a large number of coefficients G_l can be computed easily and accurately. The details are indicated in the appendix, together with numerical examples of the Mott cross section, the angular multiple scattering distribution derived from it, and data illustrating the convergence of the Legendre series. We have found it possible to include as many as 100 terms in the Legendre series before encountering clearly recognizable round-off difficulties. However, such round-off error undoubtedly occurs, and should be further investigated with the use of double-precision arithmetic.

The Goudsmit-Saunderson theory is no more difficult to evaluate than the Molière theory, and furthermore allows us to treat large deflections with increased accuracy, which is important particularly for the investigation of backscattering. A large deflection may be very rare in any one step, but yet have a good chance of occurring somewhere in a long history consisting of 100 steps. Once it occurs it has a strong influence on the subsequent history of the particle; for example, a reversal of direction, at a point not too far from the entry into a foil, greatly increases the chance of eventual backscattering from the foil. A comparison of the angular distributions predicted by the Molière and Goudsmit-Saunderson theories, particularly at large angles, is given in Table III for conditions typical of those assumed in the Monte Carlo calculations.

4. *Spatial Displacement*

Let $\Delta\xi$, $\Delta\eta$ and $\Delta\zeta$ denote the spatial displacement of the particle in a single step of the random walk, in a Cartesian-coordinate system whose ζ-axis coincides with the direction of motion of the particle at the beginning of the step. As our later applications are all limited to one-dimensional problems, we shall be concerned here only with the

change of the z-coordinate,

$$z_{n+1} - z_n = \sin\theta_n \cos\varphi_n \Delta\xi + \sin\theta_n \sin\varphi_n \Delta\eta + \cos\theta_n \Delta\zeta\,. \tag{17}$$

a. Inclusion of longitudinal and transverse displacement. The transverse displacements, $\Delta\xi$ and $\Delta\eta$, are correlated with the angular deflections ω and $\Delta\varphi$. This correlation has only been calculated in the Gaussian approximation (Rossi, 1952), with the result that (for small ω)

$$\Delta\xi = \tfrac{1}{2}\Delta s_n \left(\sin\omega \cos\Delta\varphi + k_x \sqrt{\frac{\bar{\omega}^2}{6}}\right) \tag{18}$$

$$\Delta\eta = \tfrac{1}{2}\Delta s_n \left(\sin\omega \sin\Delta\varphi + k_y \sqrt{\frac{\bar{\omega}^2}{6}}\right), \tag{19}$$

where k_x and k_y are random variables that are distributed independently according to a Gaussian distribution with mean zero and variance unity. When sampling on the basis of these formulas, one must of course exclude very large values of k_x and k_y for which $(\Delta\xi)^2 + (\Delta\eta)^2 + (\Delta\zeta)^2 > (\Delta s_n)^2$, but this has been found to be extremely unlikely. For $\bar{\omega}^2$ one can substitute $2(1 - \langle\cos\omega\rangle_{\mathrm{Av}})$, with $\langle\cos\omega\rangle_{\mathrm{Av}}$ evaluated from a more accurate theory than the Gaussian approximation. The distribution of $\Delta\zeta$ has been derived by Yang (1951) in the Gaussian small-angle approximation, and evaluated for two special situations ($\omega = 0°$, and an average over all values of ω). The evaluation of the distribution for arbitrary ω is possible but difficult. We have instead adopted a much simpler rule,

$$\Delta\zeta = \Delta s_n \frac{1 + \cos\omega}{2}\,. \tag{20}$$

This can be justified as follows: Clearly $\Delta\zeta$ cannot be greater than Δs_n, and an approximate lower bound is given by $\Delta s_n \cos\omega$. As a consequence of (15), for small Δs_n,

$$\langle\cos\omega(\Delta s_n)\rangle_{\mathrm{av}} = \exp\left\{-\int_0^{\Delta s_n} G_1(s')\,ds'\right\} \sim 1 - G_1(0)\,\Delta s_n\,. \tag{21}$$

General transport theory (Lewis, 1950) predicts that

$$\begin{aligned}\langle\Delta\zeta\rangle_{\mathrm{av}} &= \int_0^{\Delta s_n} \langle\cos(s')\rangle_{\mathrm{av}}\,ds' \\ &= \Delta s_n \frac{1 + \langle\cos\omega(\Delta s_n)\rangle_{\mathrm{av}}}{2}\,.\end{aligned} \tag{22}$$

This means that the rule (20) predicts the correct average displacement, and is an average of the upper and lower bounds of $\Delta\zeta$. Moreover, it is correct in the limit of very small ω, and remains plausible for large ω.

b. Inclusion of longitudinal displacements only. According to Eq. (17) the relative contribution of the transverse displacements $\Delta\xi$ and $\Delta\eta$ to $z_{n+1} - z_n$ can become important only when $\sin\theta_n$ is large, and even then will tend to be limited by azimuthal averaging. In problems such as reflection and transmission by foils, a particle incident normally ($\theta_0 = 0$) would have to spend a major part of its history traveling in a direction at right angles to its original direction in order for the transverse displacements to have a pronounced effect. But in this case the particle would be likely to get absorbed in the foil, so that one would expect the transverse displacements to have a small influence on reflection and transmission. It is difficult to put such considerations on a quantitative basis except by Monte Carlo calculations. Numerical experimentation, described in Section V, tends to confirm the above considerations. Therefore we have in many of our calculations set $\Delta\xi = \Delta\eta = 0$, a procedure which was also followed in the work of Hebbard and Wilson, Sidei *et al.*, and Leiss *et al.*

B. Complete Grouping, Class I′

Schemes in this class are variants of those in Class I, distinguished by the fact that the energy reached by the particle, rather than the pathlength traveled, serves as the clock for the timing of the snapshots of the particle history. Thus one preselects a set of energies, $E_0, E_1, E_2, \ldots, E_n, \ldots$, and determines the successive states of the particle as its energy drops to these values. The arbitrary preselection of energies is reasonable for protons, which can only lose a tiny fraction of their energy in an individual collision with an atomic electron (see Eq. (A13) of the appendix) and thus traverse a practically continuous range of energies. It would not be appropriate for electrons, which can lose a major fraction of their energy in a single collision so that they may jump over certain energy intervals altogether.

1. *Energy Loss*

a. Logarithmic spacing: $E_{n+1} = kE_n$.

b. Uniform spacing: $E_n - E_{n+1} =$ constant.

The advantages and disadvantages of these alternatives are the same as those of the uniform and logarithmic pathlength spacings in schemes of Class I.

2. *Pathlength*

a. Continuous slowing down approximation,

$$s_{n+1} = s_n + \int_{E_{n+1}}^{E_n} \left| \frac{dE}{ds} \right|^{-1} dE \,. \tag{23}$$

b. Consideration of pathlength fluctuations

$$s_{n+1} = s_n + \Delta s_n \,,$$

where Δs_n is distributed normally with mean

$$\langle \Delta s_n \rangle_{\mathrm{av}} = \int_{E_{n+1}}^{E_n} \left| \frac{dE}{ds} \right|^{-1} dE \tag{24}$$

and variance $\langle (\Delta s_n)^2 \rangle_{\mathrm{av}} - \langle \Delta s_n \rangle^2_{\mathrm{av}}$ (see Eq. A15 of appendix.) Small corrections to this Gaussian distribution have been derived by Lewis (1952) but we have not used them.

TABLE IV

CHARACTERISTICS OF CONDENSED PROTON HISTORY IN LEAD, MODEL I'.

a. Approximately uniform spacing on linear energy scale.

Step	Energy interval (Mev)	$\langle \Delta_s \rangle_{\mathrm{av}}$ (gm/cm^2)	p_s [a]	$\chi_c/\sqrt{B}$ [b] (degrees)
1	338.5–330.0	4.931	0.080	1.79
6	285.0–270.0	7.672	0.055	2.84
12	195.0–180.0	6.308	0.048	3.48
18	105.0– 90.0	4.100	0.038	5.12
24	20.0– 15.0	0.397	0.036	7.13
30	3.0– 2.0	0.023	0.048	10.98

b. Uniform spacing on logarithmic energy scale.

1	338.5–285.3	29.795	0.032	5.04
6	143.9–121.3	7.623	0.036	5.34
12	51.6– 43.5	1.327	0.041	5.57
18	18.5– 15.6	0.226	0.048	5.80
24	6.6– 5.6	0.040	0.059	6.11
30	2.4– 2.0	0.008	0.079	6.71

[a] p_s = per cent pathlength straggling, defined by Eq. (A17) of Appendix.
[b] $\chi_c \sqrt{B}$ is the characteristic deflection angle of the Molière theory.

After the step size and pathlength have been determined, the selection of angular deflection and spatial displacement takes place exactly as in schemes of Class I. Thus the correlation between pathlength fluctuations and multiple-scattering deflections within a step of the random walk is again disregarded. Characteristics of a condensed proton history in a lead medium are shown, by way of example, in Table IV.

C. Mixed Procedures, Class II

In this class of schemes one excludes from grouping the individual collisions (denoted as catastrophic) in which the particle loses a large fraction ϵ of its energy, greater than, say, ϵ_c. The history of the particle is divided into sections, within which no catastrophic collisions occur and in which continuous-slowing-down is assumed. Each section is terminated by a catastrophic collision. This schematization has first been applied in electron Monte Carlo calculations by Schneider and Cormack (1959), and is illustrated by Fig. 2, adapted from their paper.

Let $(E_n^a, \mathbf{u}_n^a, \mathbf{r}_n^a)$ and $(E_{n+1}^b, \mathbf{u}_{n+1}^b, \mathbf{r}_{n+1}^b)$ indicate the state of the

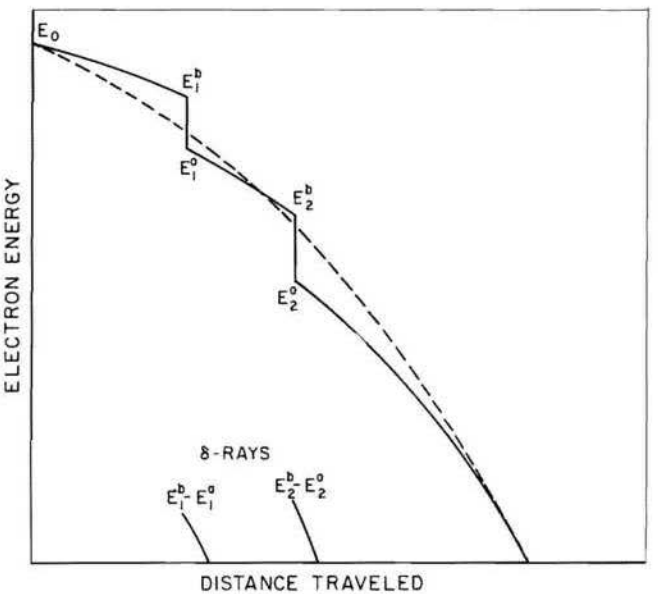

Fig. 2. Energy-pathlength plot of hypothetical electron case history. Solid curve corresponds to a Monte Carlo model of Class II with catastrophic collisions that lower the energy from E_1^b to E_1^a and from E_2^b to E_2^a and result in the occurrence of secondary knock-on electrons (delta rays). The dotted curve corresponds to the continuous-slowing-down approximation. Adapted from Schneider and Cormack (1959).

particle immediately after the nth, and immediately before the $n+1$st catastrophic collision, respectively, and let s be the pathlength between these two collisions. The pathlength distribution function is

$$P(s)\,ds = \exp\left\{-\int_0^s \mu_c(s')\,ds'\right\}\mu_c(s)\,ds\,, \tag{25}$$

where μ_c is the probability, per unit pathlength, of a catastrophic collision with energy transfer $\epsilon > \epsilon_c$. To take the energy dependence of μ_c into account, one must change from a pathlength to an energy variable, using the stopping power $|\,dE/ds\,|_{\epsilon_c}$ evaluated for all collisions with fractional energy transfer $\epsilon < \epsilon_c$. Thus

$$P(s)\,ds = e^{-Q}\,dQ\,, \tag{26}$$

where

$$Q(s) = \int_0^s \mu_c[E(s')]\,ds' = \int_{E_{n+1}^b}^{E_n^a} \mu_c(E)\left|\frac{dE}{ds}\right|_{\epsilon_c}^{-1} dE\,. \tag{26a}$$

$Q(s)$ can be interpreted as the average number of catastrophic collisions in pathlength s. The evaluation of μ_c and $|\,dE/ds\,|_{\epsilon_c}$ is described in Appendix A.

The history of a particle is traced as follows:

1. Given $E_n{}^a$, $\mathbf{u}_n{}^a$, $\mathbf{r}_n{}^a$, Q is selected from an exponential distribution and used to determine s and E_{n+1}^b.

2. A Class I (or I′) scheme (with continuous-slowing-down approximation) is applied to determine the history of the particle until the instant before the next catastrophic collision (ending with direction $\mathbf{u}_{n+1}^b$ and in position $\mathbf{r}_{n+1}^b$).

3. The magnitude of the fractional energy loss ϵ in the $n+1$st catastrophic collision is sampled from the appropriate single-scattering distribution $g(\epsilon;\epsilon_c)$ [see Eq. (A4) of the appendix].

4. The catastrophic collision leaves the position of the particle unchanged, i.e., $\mathbf{r}_{n+1}^a = \mathbf{r}_{n+1}^b$. The energy of the particle is reduced from E_{n+1}^b to

$$E_{n+1}^a = E_{n+1}^b(1-\epsilon)\,. \tag{27}$$

Associated with this energy loss is a deflection through an angle $\omega'(\epsilon)$ completely determined by conservation of momentum and energy in the collision [see Eq. (A3) of the appendix]. The new direction, $\mathbf{u}_{n+1}^a$ is determined by the customary trigonometric relations

$$\cos\theta_{n+1}^a = \cos\theta_{n+1}^b\cos\omega' + \sin\theta_{n+1}^b\sin\omega'\cos\Delta\varphi'\text{, etc.,} \tag{28}$$

where $\Delta\varphi'$ is an angle randomly distributed between zero and 2π.

5. The catastrophic collision leads to a secondary knock-on electron with energy $E_0 = E^b_{n+1}\epsilon$, whose direction is also determined by the kinematics of the collision, and whose history can be followed in turn.

A small set of corresponding E-, s- and Q-values for electrons in aluminum is shown in Table V. It illustrates the dependence of the mean

TABLE V

PROBABILITY OF ELECTRON-ELECTRON COLLISIONS WITH FRACTIONAL ENERGY LOSSES GREATER THAN ϵ_c, IN ALUMINUM MEDIUM.

	$\epsilon_c = 0.1$		$\epsilon_c = 0.03$		$\epsilon_c = 0.01$	
E (Mev)	s gm/cm²	$Q(s)$	s gm/cm²	$Q(s)$	s gm/cm²	$Q(s)$
1.0	0.0000	0.0000	0.0000	0.0000	0.0000	0.0000
0.5	0.3602	0.3391	0.3893	1.4610	0.4211	5.0390
0.25	0.5186	0.6920	0.5617	3.0509	0.6091	10.6461
0.125	0.5795	1.0677	0.6286	4.8000	0.6829	16.9308
0.0625	0.6004	1.4790	0.6518	6.7577	0.7088	24.0852

number of catastrophic collisions, Q, on the cutoff parameter ϵ_c (in the range $0.01 \leqslant \epsilon_c \leqslant 0.1$, which we have found useful in later calculations). In the limiting case $\epsilon_c = \frac{1}{2}$ (for electrons) one is led back to a Class I scheme, with complete grouping, whereas the other limiting case, $\epsilon_c = 0$, corresponds to a conventional Monte Carlo calculation in which all individual collisions are sampled. It is of course not necessary to use the same value of the cutoff parameter throughout the history of a particle; for example, one may require that those catastrophic collisions are singled out, in which an amount of energy greater than $\mathbf{E}_c$ is lost, so that $\epsilon_c = E_c/E$.

Among the advantages of Class II over Class I are the following: The initial state of secondary knock-on electrons is indicated unambiguously, angular deflections due to inelastic scattering can be calculated more accurately, and the correlation between energy-loss fluctuations and multiple scattering deflections is preserved more faithfully. On the other hand, the random occurrence of catastrophic collisions allows less storing of predigested transition probabilities for the condensed random walk, so that the computations become more laborious (see Section IV). It is possible to extend the Class II procedures to angular deflections, excepting from grouping all collisions associated with deflections greater than a cutoff angle ω_c. In problems where such individual collisions

can make important contributions, as is the case of the backscattering of electrons from foils, this might be advantageous, but has not yet been tried.

IV. Computational Aspects

A. Random Sampling

Once a particular Monte Carlo scheme for condensed histories has been chosen, the required random sampling techniques are similar to those in conventional Monte Carlo calculations.

Many random numbers are needed, which must be uncorrelated and distributed uniformly between zero and one. We have used the well-known method of congruential multiplication, adapted to an IBM 704 computer, according to which so-called pseudorandom numbers ρ_n are generated by the following scheme:

$$\begin{aligned} j_0 &= c \\ j_{n+1} &= 5^d j_n \bmod 2^{35}, \\ \rho_n &= 2^{-35} j_n \end{aligned} \tag{29}$$

where c and d are odd integers. Two types of sequences were employed. The main sequence, started with an arbitrary c and continued with a multiplicative factor 5^{11}, provided the starting number c for successive histories. In each history, the sequence thus started was continued with a multiplicative factor 5^{13}. This procedure was set up in order to facilitate "correlated" sampling. By this we mean comparison calculations, for example of the backscattering of electrons and positrons, in which two sets of histories are generated, one for electrons and the other for positions, each set using insofar as possible the same sequences of random numbers. Observed differences of backscattering are then only the result of differences in the scattering cross sections, and irrelevant statistical fluctuations are reduced. The use of main and secondary pseudorandom number sequences as described above has the advantage that one can produce sets of matched pair electron and positron histories such that each member of a pair, insofar as it is of the same length, will be based on exactly the same sequence of random numbers as its mate. This procedure can be applied not only to electron-positron differences, but also to the investigation of the different Monte Carlo models.

Many ingenious methods are available for sampling random variates x

from a distribution $f(x)$ with the use of pseudorandom numbers (see, e.g., H. Kahn, 1954). Many of them were developed when the memory capacity of computers was quite limited. The large capacity (typically 32,000 words) of present-day computers makes it preferable to use a less ingenious method which wastes memory space but can be carried out faster, by relying on the use of the cumulative probability distribution

$$F(x) = \int_{-\infty}^{x} f(x')\, dx' . \tag{30}$$

F is a random variable distributed according to

$$P(F) = f(x)\frac{dx}{dF} = 1 . \tag{31}$$

In other words, F is distributed uniformly between zero and one. One thus chooses a random number ρ, sets $F(x) = \rho$ and solves for $x = F^{-1}(\rho)$. This can easily be done with a table-look-up, provided one stores a large table of $F(x)$ in the computer memory. One procedure which has been found convenient is the following:

1. Compute $F(x_n)$ for a dense set of x-values spanning the range of $f(x)$.
2. By interpolation, find a set of x-values such that

$$F(\tilde{x}_m) = (m - \tfrac{1}{2})/M. \qquad m = 1, 2, \cdots, M$$

Store the $\tilde{x}_m$'s in the computer memory. They constitute, in good approximation, a set of "equally probable" variates from which one can make a selection.

3. To sample from $f(x)$, pick a random number ρ, and compute i = integral part of $M\rho$. The desired random variate is $\tilde{x} = x_i$. An equivalent but faster procedure, which cannot be done in FORTRAN language, is to use a section of the random number, in binary form to indicate the value of the address i. This requires M to be a power of 2.

Suppose we want so sample a random variate $\cos \Delta\varphi$, where $\Delta\varphi$ is an angle distributed with equal probability between 0 and π. If we are satisfied to specify $\Delta\varphi$ to the nearest degree, it is then sufficient to store in the computer memory 180 numbers ($\tilde{x}_m = \cos[(m - \frac{1}{2})\,\pi/180]$, $m = 1, 2, \ldots, 180$) and each selection requires the generation of one random number, one multiplication and a truncation of the product. This procedure can be compared with a more ingenious "rejection technique" which requires only a very few memory cells but more arithmetic.

1. Select a pair of random numbers, ρ_1 and ρ_2.
2. If $\rho_1^2 + \rho_2^2 \leqslant 1$, set $\cos \Delta\varphi = (\rho_1^2 - \rho_2^2)/(\rho_1^2 + \rho_2^2)$.

3. If $\rho_1^2 + \rho_2^2 > 1$, pick another pair of random numbers and try again. The probability of accepting a pair of random nubmers is $\pi/4$, so that on the average one must generate 2.55 random numbers, and perform 2.55 multiplications and one division, to select one value of $\Delta\varphi$.

The various statistical techniques such as biased sampling, importance sampling, Russian roulette, etc., which have been developed for application to gamma-ray or neutron transport problems also are applicable to condensed charged-particle histories. In other words, one could manipulate the rules of the game so as to increase the relative likelihood of interesting but ordinarily rare events such as penetration through a very thick foil.

In the present paper, the technique of correlated sampling, already touched upon in Section IV, A and further described in Section V, A, was used to obtain greater precision when comparing backscattering and transmission under slightly different conditions (e.g., for electrons and positrons). Particle histories were of course dropped as soon as they reached a stage where no further contribution to the problem at hand could be expected, for example, when electrons had penetrated so deep into a semiinfinite medium that their residual range was too small for reemergence, or when the residual electron displacement could not remove them from a layer of the medium in which energy dissipation was to be determined.

More elaborate variance-reducing techniques were not used in this paper, for a number of reasons. First, many of the problems under consideration, such as backscattering, transmission through foils of moderate thickness, and the spatial distribution of energy dissipation did not involve particularly rare events. Second, the Monte Carlo models were often not refined enough for the accurate calculation of extremely deep penetration for which statistical elaborations would have been most effective. Third, an increase of computing efficiency was often achieved through the use of the same set of histories for the simultaneous solution of several problems (i.e., reflection and transmission by a set of foils with different thicknesses) in which case the same biasing would not have been appropriate for all of them. However, it must be admitted that considerable computational economies in charged-particle Monte Carlo problems could be achieved thrcugh the use of more sophisticated sampling techniques.

B. Flow and Arrangement of the Computations

The remarks in this Section are based on the author's experience in programming a variety of exploratory calculations in FORTRAN

language for an IBM 704 computer with a memory of 32768 words. Three main types of programs were needed: (1) A *Data Preparation Program* which pre-computes transition probabilities for condensed random walks; (2) A *Main Program* which generates Monte Carlo case histories and applies them to particular problems, and (3) A *Processing Program* which combines and analyzes the results obtained in various runs of the Main Program. Depending on the Monte Carlo model, different groups of such programs had to be written. Usually one Data Preparation Program was sufficient to provide input for a whole set of Main Programs. The Data Preparation Program was the most difficult and time-consuming to develop but had a running time of only a few minutes on the IBM 704. The Main Program was usually short and easy to code, but consumed large amounts of machine time, being largely repetitive. The Processing Program required relatively little programming or machine effort, and was needed to rescue the author from a flood of output data.

1. *Data Preparation Program*

The purpose is to make the random sampling in the Main Program as fast and painless as possible. This is achieved primarily through the tabulation of cumulative probability distributions, or related quantities, so that the sampling requires only a table-look-up but no further arithmetic. As an example, let us consider the generation of electron histories according to a model of Class I, assuming logarithmic spacing, the continuous-slowing-down approximation for energy loss, and the use of the Goudsmit-Saunderson multiple-scattering angular distribution together with the Mott scattering cross section. We assume further that the sampling of angular deflections is to be carried out with the use of a set of "equally probable" angles, as described in Section IV, A. The required program can be characterized by its input, function, and output. The *input* must specify:

(1) Properties of the medium (atomic number and weight, mean ionization potential, etc.).

(2) Details of the Monte Carlo model, including the spacing parameter k.

(3) The energy span to be covered, and the number of "equally probable angles" to be used for sampling.

The *function* of the program is to compute:

(1) The energies corresponding to each step.

(2) The mean energy loss rate by ionization.

(3) The pathlength for each step, from (1) and (2).

(4) The Mott scattering cross section at each energy.

(5) The cumulative Goudsmit-Saunderson multiple-scattering angular distribution, from (4).

(6) A table of "equally probable" scattering angles for each step, derived from (5).

The *output* of the programs consist of tables of items (1), (3), and (6) above. For example, if we require 96 steps which reduce the energy in steps of $2^{-1/16}$ from E_0 to $E_0 2^{-6}$, and 40 equally probable angles at each energy (these magnitudes are typical for some of our later calculations), then the output will comprise approximately 4000 numbers, which are loaded on tape or punched cards for later use, and also printed out to allow inspection and checking.

Now suppose that we drop the continuous-slowing-down approximation and decide to sample energy losses from a Landau distribution. We must then tabulate a set of "equally probable" values of the Landau's universal parameter λ [see Eq. (A17) of the appendix] from which the energy loss in each step can be obtained by simple arithmetic. A more severe complication arises from the fact that the Goudsmit-Saunderson angular distribution depends not only on the pathlength of the step but also on the energy of the particle at the beginning of the step which in the previous example was determined in advance but now is subject to statistical fluctuations. Thus the angular distribution at each step must be tabulated for at least a small set of initial energies, so that interpolation becomes possible. In Class II models, where even the pathlength per step is statistical rather than predetermined, more tabulations are necessary, and the amount of data per step may be several times larger than that required for the simplest model (Class I, continuous-slowing-down approximation). The author has no experience with data input greater than 12,000 words per problem. However, there is no doubt that with the magnetic tape input facilities of modern computers even much larger amounts of data can easily be fed into the Main Program, provided the latter is arranged to accept them in convenient form.

2. *Main Program*

We shall indicate the flow of the calculation for two types of Main Program, the first of which generates Monte Carlo case histories in series, one after the other, and is applicable to problems with a limited amount of data input whereas the second type generates many histories

simultaneously, in parallel, and is appropriate when the data putin is very large. In the description we shall assume, for the sake of concreteness, that the problem to be solved is the transmission and reflection of particles by foils.

a. Series arrangement. The following breakdown indicates the logic of the program, but does not necessarily correspond in all details to the actual machine program.

(1) *Setup of Problem.* This is the main routine which links together the other subroutines listed below. It requires input parameters that specify the properties of the medium and of the diffusing particle, the characteristics of the Monte Carlo model, the number of histories to be sampled, the conditions for terminating a history, the configuration of the medium (i.e., the foil boundaries), etc.

(2) *Input Data.* If the required input data have previously been generated, they are read into the computer memory from magnetic tape. If not, the *Data Preparation Program* is put in operation, and the resulting tabulations are stored in the memory and also on magnetic tape for possible future use.

(3) *Start of History.* A history is begun by specifying the initial position, energy, and direction of the particle.

(4) *Advance.* The particle is allowed to make one step of the condensed random walk, selected with the use of the tabulated input data.

(5) *Scoring.* If the particle, as the result of the step just taken, crosses a foil boundary of interest, the energy and direction of escape, and the identifying label of the boundary are recorded.

(6) *Termination of History.* If the particle can no longer escape from the foil, or if some other condition for termination has been satisfied, one proceeds to subroutine (7). Otherwise, one proceeds to subroutine (4) and lets the particle take another step.

(7) *Termination of the Problem.* If the desired number of histories has been sampled, one proceeds to subroutine (8). Otherwise, one proceeds to subroutine (3) and starts another history.

(8) *Output.* Summary information is computed and printed out, such as reflection and transmission coefficients. This serves mainly as "quality control" indicating that the program has been running satisfactorily. The detailed information produced by the scoring subroutine is dumped on magnetic tape and provided with an identifying label so that it can be recovered easily for later use in a Processing Program.

b. Parallel arrangement. This requires a modification of the series program as follows: Initially, the input-data read into the computer memory are limited to a small energy range, extending from the highest particle energy to be considered down to an intermediate energy. Not just one but many histories are started and followed together until they are either terminated or go out of the energy range of the input data. When a history goes out of range, the position, energy, and direction of the particle are stored to allow later continuation. After the entire group of histories has been processed in this manner, another input-data set is read into the memory which covers a lower energy interval and replaces the old input data set in exactly the same memory location, which is permissible because the old set will not be needed again.

The histories which previously went out of range are now continued with the use of the new data. This procedure is repeated until the entire energy range of interest has been covered. Compared to a series program, some additional memory space is required to record the characteristics of histories that must be continued, but much less space is required for the storage of input data.

c. Computing time. The work for this paper was done with a great variety of experimental programs which were sometimes changed from run to run, so that it is not easy to arrive at exact time estimates. The preponderant amount of computing effort goes into the execution of the two subroutines *Advance* and *Scoring* which constitute the innermost loops of the Main Program. Time estimates can therefore be made in terms of the unit time required for doing one step of the random walk and analyzing its effects. This unit time must then be multiplied by the number of steps in a condensed history and the number of histories sampled. The total time per problem is equal to this product increased a few percent to allow for the execution of the other subroutines.

Depending on the complexity of the Monte Carlo scheme the unit time per step has been found to range from 5 to 12 milliseconds of IBM 704 time. With an IBM 7090 computer this time would be reduced by a factor between five and six.

3. *Processing Program*

It may, under some circumstances, be possible to achieve great computational economy by generating a set of Monte Carlo histories without regard to the conditions of any particular problem, storing them, and using them repeatedly later for various applications. (This would require a shift of the Scoring subroutine from the Main Program

to the Processing Program.) Whether this is practical or not depends on the relative speed with which histories can be computed or read into and out of the computer memory. In a calculation with a desk-computer, the production of histories is quite laborious, whereas note-books provide a large and easily accessible memory so that the reuse of histories is advantageous. This has been demonstrated by Sidei, *et al.* (1957) who efficiently reused different portions of a set of a few hundred Model-I histories to determine the transmission of electrons as a function of the incident energy and the albedo as a function of the source obliquity. When computers are used, the sample size tends to increase greatly and a vast amount of information must be transferred. For example, if 5000 histories of 50 steps are each generated, and three numbers (energy, direction, position) are recorded for each step, approximately 7.5×10^5 words have to be stored, which requires several hundred feet of magnetic tape. To calculate these numbers in the first place would take on the order of, say, 250 to 500 seconds, on an IBM 7090 computer. With the fasted tape equipment available for use with this computer, at most 10,000 words per second can be transferred from or to tape, so that at least 75 seconds would be required for recording the histories on tape. Actually, the time would be considerally longer, because the information would have to be organized in suitable blocks, separated by gaps on the magnetic tape, which would slow up the transfer of information. On the other hand, computers of very modern design, such as the IBM 7090, can simultaneously accept information from tape and perform arithmetic operations, which would make the tape read-in less of a burden. The relative merits of repeated use as recalculation of histories can only be decided with detailed knowledge of the characteristics of the computer and its associated input-output equipment, and is one which the author does not feel competent to answer. In any case, the error-free processing of such vast amounts of information would require an elaborate checking and indexing procedure involving a very substantial additional programming effort.

In the present work, histories were used in one run on the machine for the solution of several problems, which resulted in time savings up to 50% but led to the difficulty that there was not enough memory space for storing the various energy spectra, angular distributions, and other information to be printed out at the end of the run. This difficulty was overcome by recording, on binary cards or on magnetic tape, the details of a history whenever some event of interest occurred. For example, when the particle crossed one of many possible foil boundaries, the identifying number of the boundary, together with the

energy and direction of the escaping particle, was compressed into one binary word, and when a sufficient number of these words had accumulated they were stored on tape or cards. If 5000 histories are to be applied to 5 problems, and if in each history one interesting event occurs for each problem (a considerable overestimate), only 25,000 words have to be stored, which presents no problem.

The function of the processing routine was then to combine the compressed information recorded in various runs of the Main Program, to normalize the results, compute reflection and transmission coefficients, evaluate their statistical accuracy, obtain energy spectra and angular distribution histograms by suitable classification, and so on. This took only a very short time, so that it was practical to repeat the processing whenever a new output format, or a new spectral classification, or some other additional information was desired.

V. Solution of Typical Problems

With one exception, the problems discussed in this section deal with charged particles whose energy is so low that radiative energy losses can be neglected. This reflects the state of the literature as well as the desire to confine the discussion to Monte Carlo calculations in which the use of condensed particle histories is essential. At extremely high energies, where bremsstrahlung and the resulting electron-photon cascade are of prime importance, multiple Coulomb scattering is a minor effect that is often treated approximately, without the more elaborate procedures required at lower energies. For example, very extensive Monte Carlo calculations of electron-photon cascades at energies up to 20 Bev have been made by Butcher and Messel (1960) in which the generation and transport of photons were treated by conventional sampling (without the grouping of collisions), and in which the Coulomb interactions of electrons were considered only as giving rise to a constant energy loss per unit pathlength. There is a need for further Monte Carlo calculations at intermediate energies, between, say, two Mev and several hundred Mev, in which both bremsstrahlung and charged-particle penetration are treated accurately.

In the review of previous work,[1] and of new calculations by the author, it will be necessary to specify the methods used for constructing

[1] The author has learned, after completion of this article, that J. F. Perkins has made extensive Monte Carlo calculations of electron backscattering and transmission, by schemes of Class I, based on the use of the Molière and Landau distributions. Unfortunately it was too late to include this material in the review.

TABLE VI

SUMMARY OF CLASS I MONTE CARLO MODELS OF CONDENSED HISTORY.

Procedure	Symbol
Pathlength	
a. Logarithmic spacing	PL
b. Mixed logarithmic spacing	PLM
c. Uniform spacing	PU
Energy loss	
a. Continuous-slowing-down approx.	EC
b. Fluctuations of ionization loss	EI
c. Fluctuations of ionization and bremsstrahlung loss	EIB
Angular deflection	
a. Gaussian approximation	AG
b. Molière theory	AM
c. Goudsmit-Saunderson theory	AGS
Displacement	
a. Longitudinal and transverse displacement	DLT
b. Longitudinal displacement only	DL

condensed particle histories. Table VI summarizes the procedures for schemes of Class I, the class which has found most frequent use, and assigns to each procedure a symbol. The symbols will be used in an abbreviated notation to identify the origin of results in figures and tables. For example, the notation

$$\text{Model } \{I, PL(16, 96), EC, AM, DLT\}$$

indicates the use of a Class I scheme; it means that the pathlengths for successive steps were selected with a logarithmic spacing such that $k = E_{n+1}/E_n = 2^{-1/16}$; that 96 steps were followed in each history (unless the history was terminated earlier through escape of the particle from the medium); that energy loss was calculated according to the continuous-slowing-down approximation; that angular deflections were sampled from the Molière distribution and that longitudinal as well as transverse multiple-scattering displacements were taken into account.

To take another example, the notation

$$\{\text{Model } I, PLM(16/8, 48), EI, AGS, DL\}$$

means that pathlengths were selected according to a mixed logarithmic

scheme, with $k = 2^{-1/16}$ in the interior of the medium and with a reduced spacing $k = 2^{-1/16\times 8} = 2^{-1/128}$ in the neighborhood of a boundary; that the history was followed through no more than 48 steps with the larger spacing; that fluctuations of energy loss by ionization were taken into account; that the Goudsmit-Saunderson angular distribution was used, and that only longitudinal displacements were considered. Unless the contrary is stated, the Goudsmit-Saunderson distribution was evaluated with the Mott scattering cross section.

The penetration of charged particles, under the assumption of continuous-slowing-down, is governed by an approximate scaling law. Let z denote the depth of penetration from the source, and

$$r_0 = \int_0^{E_0} \left| \frac{dE}{ds} \right|^{-1} dE \tag{32}$$

the mean range at the source energy E_0. When the spatial distribution of the diffusing particles is expressed in terms of the ratio z/r_0, the shape of the distribution is insensitive to the value of E_0, provided E_0 is smaller than twice the rest energy of the particles. This is a consequence of the scaling law for angular multiple-scattering deflections mentioned earlier [Eq. (6)], according to which the mean cosine of the deflection angle depends, to first order, only on the ratio of the energies of the particle at the end and the beginning of the path traversed, or —equivalently—on the ratio of the corresponding mean residual ranges. Taking advantage of the scaling law, we shall extend the generality of many of the Monte Carlo results by expressing them as functions of z/r_0. A small set of r_0-values for aluminum and gold, obtained with the use of Eqs. (A9-11), are given in Table VII. Many of the calculations to be discussed are for these materials which are representative of low-Z and high-Z materials.

TABLE VII

MEAN RESIDUAL RANGE, r_0, OF ELECTRONS AND POSITRONS (gm/cm²).

E_0 (Mev)	Aluminum, I = 163 ev		Gold, I = 797 ev	
	electrons	positrons	electrons	positrons
2.0	1.237	1.259	...	...
1.0	0.5568	0.5598	...	...
0.5	0.2258	0.2237	0.3451	0.3406
0.25	0.08196	0.07946	0.1288	0.1236
0.125	0.02706	0.02565	0.04372	0.04068
0.0625	0.008385	0.007778	0.01390	0.01256

In various tables the estimated errors of the results are shown. These are standard deviations indicating the statistical accuracy of the Monte Carlo calculations. Systematic errors will be discussed separately.

A. Backscattering of Electrons and Positrons

1. *Albedo*

The most important parameter characterizing backscattering is the total probability of reflection which is often called the *albedo*. Alternatively, the albedo may be defined as the ratio of the reflected to the incident current. The albedo of a foil increases with foil thickness until a saturation value is reached. In Table VIII some Monte Carlo

Table VIII

Dependence of Electron Backscattering on Foil Thickness[a].

Foil thickness	Ratio of foil albedo to semi-infinite-medium albedo	
z/r_0	aluminum[b]	gold[c]
0.025	...	0.16
0.05	0.07	0.43
0.10	0.23	0.83
0.15	0.43	0.97
0.20	0.71	1.00
0.25	0.89	...
0.30	0.98	...
0.35	1.00	...

[a] 0.5-Mev electrons incident perpendicularly on foil.
[b] Based on 5000 histories generated according to Model {I, PL(16, 48), EC, AGS, DL}.
[c] Based on 2000 histories generated according to Model {I, PL(32, 96), EC, AGS, DL}.

results are given which illustrate the approach to saturation backscattering for 0.5-Mev electrons incident perpendicularly on a foil. Complete saturation is reached with gold foils when $z/r_0 = 0.20$ and with aluminum foils when $z/r_0 = 0.35$. This implies that electrons are turned around sooner in gold than in aluminum, which corresponds to the fact that the mean angular deflection, over a pathlength with given fractional energy loss, increases with the atomic number of the medium. In the backscattering problems to be discussed from now on, the foil will be assumed to have saturation thickness, so that the albedo is a function of the source energy and direction of incidence only.

Figure 3 gives a comparison of the calculated and experimental values of the albedo, for perpendicular incidence on aluminum, as a function of the source energy. There is fair agreement, even through the Monte

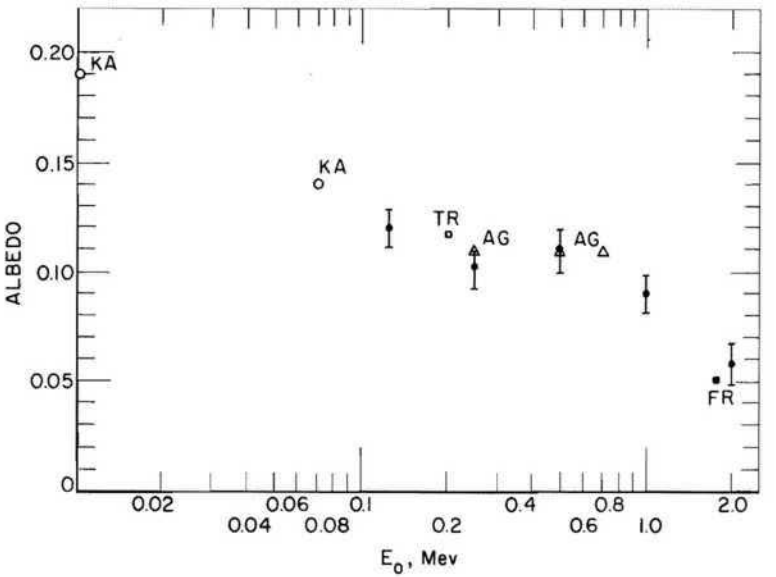

FIG. 3. Albedo as function of the source energy E_0, for electrons incident on a semi-infinite aluminum medium. Results of several experiments are given by: o KA, Kanter (1957); Δ AG, Agu *et al.* (1958a); TR, Trump and Van de Graaf (1949); FR, Frank (1959). Monte Carlo, 1000 histories for each source energy E_0, generated according to Model {I, PL (16, 96), EC, AM, DLT}.

TABLE IX

ELECTRON ALBEDO OF SEMI INFINITE ALUMINUM MEDIUM.[a]

E_0	θ_0					
(Mev)	0°	45°	60°	75°	90°	Isotropic
2.0	0.059	0.159	0.284	0.457	0.790	0.317
1.0	0.090	0.220	0.333	0.494	0.796	0.357
0.5	0.109	0.229	0.316	0.494	0.782	0.363
0.25	0.097	0.238	0.361	0.531	0.798	0.384
0.125	0.121	0.236	0.348	0.518	0.788	0.369

[a] Based on 1000 histories for each source energy E_0, calculated according to Model {I, PL(16, 96), EC, AM, DLT}. Standard deviation of albedo A is $\sqrt{A(1-A)/1000}$.

Carlo results are based on a relatively small sample of 1000 histories for each value of E_0, obtained by a very simple scheme of Class I. In Table IX is an extension of the calculated values to the case of oblique incidence, ranging from $\theta = 0°$ (perpendicular incidence) to $\theta = 90°$ (grazing incidence). The obliquity-dependence of the albedo is rather independent of the source energy, and is consistent with measurements by Kanter (1957) at energies between 10 and 70 kev. Table IX also gives albedo values for isotropic incidence (with $\cos\theta_0$ distributed uniformly between 0 and 1), which agree with measurements by Kanter (1957) with an Rb^{187} beta-ray source (max. energy 0.275 Mev), and with measurements by Suzor and Charpak (1952) with several different beta-ray sources (max. energies between 0.17 and 1.7 Mev), but are approximately 10% lower than results of Seliger (1952) with a P^{32} beta-ray (maximum energy 1.7 Mev).

2. *Albedo Comparisons*

a. Electron-positron albedo differences. To estimate such difference we have used the technique of correlated sampling. Pairs of electron and positron histories were sampled, both members of each pair being generated with the same sequence of random numbers insofar as possible.

To every electron history we assign a variable α_E which is equal to 1 if the electron is reflected and 0 otherwise, so that the electron albedo A_E is equal to the mean value $\overline{\alpha_E}$, taken over all sampled histories. A similar variable α_p is assigned to each positron history such that the positron albedo A_p is equal to $\overline{\alpha_p}$. The variances of α_E and α_p are

$$\sigma_E^2 = \overline{\alpha_E}(1 - \overline{\alpha_E}) \tag{33}$$

$$\sigma_P^2 = \overline{\alpha_P}(1 - \overline{\alpha_P}), \tag{34}$$

and their correlation coefficient (which must lie between -1 and $+1$) is

$$\rho(\alpha_E, \alpha_P) = \frac{\overline{\alpha_E\alpha_P} - \overline{\alpha_E} \cdot \overline{\alpha_P}}{\sigma_E\sigma_P}. \tag{35}$$

The quantity to be estimated is the ratio of the electron albedo to the positron albedo, A_E/A_p. The fractional standard deviation of the estimate of this ratio is

$$\delta = \frac{1}{\sqrt{N_0}} \left\{ \left(\frac{\sigma_E}{\overline{\alpha_E}}\right)^2 - 2\rho \frac{\sigma_E\sigma_P}{\overline{\alpha_E} \cdot \overline{\alpha_P}} + \left(\frac{\sigma_P}{\overline{\alpha_P}}\right)^2 \right\}, \tag{36}$$

where N_0 is the number of histories sampled. The larger the correlation coefficient, the smaller is the statistical error.

By way of example, Table X contains a classification of 10,000 pairs

TABLE X

ANALYSIS OF CORRELATED ELECTRON AND POSITRON HISTORIES.[a]

		Electrons		
		Reflected	Absorbed	Subtotal
Positrons	Reflected	891	46	937
	Absorbed	165	8898	9063
	Subtotal	1056	8944	10000
				Total

[a] Based on 10 000 electron and positron histories, generated according to Model {I, PLM (16/8, 48), EC, AGS, DL}, for a source energy of 0.5 Mev and perpendicular incidence on a semi infinite aluminum medium.

of correlated electron and positron histories, from which the following information can be obtained.

$$\overline{\alpha_E} = 0.1045;\ \overline{\alpha_P} = 0.0937;\ \overline{\alpha_E}/\overline{\alpha_P} = 1.127;$$
$$\sigma^2(\alpha_E) = 0.0944;\ \sigma^2(\alpha_P) = 0.0849; \tag{37}$$
$$\overline{\alpha_E \alpha_P} = 0.0891;\ \rho(\alpha_E, \alpha_P) = 0.885\,.$$

When these numbers are substituted into Eq. (36) one finds that the fractional standard deviation δ has the value 0.016. If the correlation coefficient were zero rather than 0.885, the value of δ would be 0.043. With the statistical error inversely proportional to $\sqrt{N_0}$, the use of correlated sampling in the example has therefore increased the effective

TABLE XI

COMPARISON OF ELECTRON AND POSITRON ALBEDO.

Medium	E_0 (Mev)	θ_0	Ratio of electron to positron albedo
Aluminum[a]	1.0	0°	1.08 ± 0.01
Aluminum[a]	1.0	Isotropic	1.01 ± 0.02
Aluminum[b]	0.5	0°	1.12 ± 0.02
Aluminum[b]	0.5	Isotropic	1.02 ± 0.01
Gold[c]	0.5	0°	1.20 ± 0.03
Gold[c]	0.5	Isotropic	1.09 ± 0.02

[a] 1000 histories, Model {I, PL (16, 96), EC, AGS, DLT}.

[b] 10,000 histories, $\theta_0 = 0°$; 3,000 histories, isotropic source } Model {I, PLM (16/8, 48), EC, AGS, DL}.

[c] 5,000 histories, Model {I, PL(32, 96), EC, AGS, DL}.

sample size by a factor $(0.043/0.016)^2 = 8.2$, without any increase in computation.

Table XI contains ratios of the electron albedo to the positron albedo, for aluminum and gold and various source energies. Electrons are backscattered more than positrons. The difference increases with the atomic number of the medium and is due mainly to the behavior of the Mott scattering cross section at large angles (see Table XIX) and of the corresponding multiple scattering angular distributions (see Tables III, XXII and XXIII).

The only experimental determination of the electron-positron backscattering difference appears to have been made by Seliger (1952) with isotropic sources (electrons from P^{32} with a maximum energy of 1.7 Mev, positrons from Na^{22} with a maximum energy of 0.58 Mev). As shown in Table IX, the albedo increases slowly with decreasing source energy. Seliger's results might thus be expected to result in an underestimate of the electron-positron albedo ratio because the average energy of his electrons was higher than that of his positrons. In fact, however, his ratios are 1.4 for aluminum and 1.3 for gold, and are much higher than the calculated ratios, particularly for aluminum. By allowing for the possibility of annihilation in flight, the calculated positron albedo would be reduced by approximately 1%, which is far too little to remove the discrepancy. It does not seem likely that further refinements of the Monte Carlo method will lead to significantly different results so that additional experiments would be desirable to clarify the situation.

An estimate of the electron-positron albedo ratio has also been made by Miller (1951) who evaluated a simple albedo theory of Bothe (1949) with the use of the Mott scattering cross section. Miller found a ratio 1.16 for 0.5-Mev electrons and positrons incident on mercury ($Z = 80$), for a source geometry intermediate between isotropic and perpendicular incidence. This is in good agreement with the results in Table XI for gold.

b. Model differences. Table XII illustrates how the calculated albedo depends on the type of multiple-scattering theory used to select angular deflections in the construction of condensed histories. The data in the table were obtained by correlated sampling, and the correlation coefficient ρ relating any two calculations was found to be of order 0.8. With a sample of 1,000 histories, the ratio of albedos for two different assumed angular distributions has a fractional standard deviation approximately equal to $0.1\sqrt{2(1-\rho)} \sim 0.06$. Thus the albedo comparisons are not statistically conclusive, but they do show trends that conform to one's expectations. Possibly significant differences occur only for perpendicular

TABLE XII

DEPENDENCE OF CALCULATED ELECTRON ALBEDO ON MODEL OF CONDENSED RANDOM WALK[a]

Model Characteristics	Albedo	
	$\theta_0 = 0$	Isotropic source
[b]	0.086 ± 0.009	0.367 ± 0.015
[c]	0.100 ± 0.009	0.476 ± 0.015
[d]	0.090 ± 0.009	0.357 ± 0.015
[e]	0.088 ± 0.009	0.355 ± 0.015

[a] For 1-Mev electrons incident perpendicularly on a semiinfinite aluminum medium. Based on 1000 histories.

[b] Model {I, PL (16, 96), EC, AGS (Mott), DLT}.

[c] Model {I, PL (16, 96), EC, AGS (Rutherford), DLT}.

[d] Model {I, PL (16, 96), EC, AM (Molière), DLT (long. and transv.)}.

[e] Model {I, PL (16, 96), EC, AM (Molière), DL (long. only)}.

but not for isotropic incidence. This is plausible because the multiple-scattering theories differ mainly in their predictions concerning large angular deflections, and such deflections play an important role in promoting backscattering only when the direction of incidence is more or less perpendicular. The use of the Rutherford instead of the Mott cross section leads to an overestimate of backscattering that is expected from the small value of $\sigma(\text{Mott})/\sigma(\text{Ruth})$ at large angles. Finally, Table XII indicates that the neglect of the transverse multiple scattering displacements has no significant effect on the calculated value of the albedo.

Table XIII is concerned with the influence of stepsize on the calculated

TABLE XIII

DEPENDENCE OF CALCULATED ELECTRON ALBEDO ON STEP-SIZE OF CONDENSED RANDOM WALK[a]

Step-size and number of steps	Albedo
PL (4, 24)	0.083 ± 0.006
PL (8, 48)	0.092 ± 0.006
PL (16, 96)	0.108 ± 0.007
PL (32, 192)	0.119 ± 0.007
PLM (16/8, 96)	0.108 ± 0.006

[a] For 0.5-Mev electrons incident perpendicularly on a semiinfinite aluminum medium. Based on 5000 histories generated according to Model {I, PL, EC, AGS, DL}.

albedo. The latter increases slowly as the steps are made smaller and eventually appears to reach a limiting value, not far from the stepsize $k = 2^{-1/16}$ for aluminum which was used in many of the calculations. The underestimate of the albedo for large stepsize is presumably connected with the approximate treatment of spatial displacements in Monte Carlo schemes of Class I, the particles being allowed to penetrate too deep into the medium before being given a chance to turn around and reemerge. In this situation, the use of mixed logarithmic spacing is advisable, with fine steps near the boundary.

3. *Angular Distribution of Backscattered Electrons*

Whereas in a conventional Monte Carlo treatment, with assumed rectilinear propagation between collisions, there is no ambiguity regarding the direction with which a particle crosses a boundary of interest, this is not so for condensed histories. Suppose the crossing of the boundary $z = 0$ of a semiinfinite medium occurs in the nth step. One then merely knows the states (E_n, θ_n, z_n) and $(E_{n+1}, \theta_{n+1}, z_{n+1})$ at the beginning and end of the step, and must guess the direction θ_B at the intermediate position $z = 0$. Most authors have simply used the direction at the beginning of the step, setting $\theta_B = \theta_n$. However, when average multiple scattering deflections per step as large as 10 to 25° are allowed, a better approximation is desirable. In principle one should sample θ_B from an appropriate probability distribution, which is available only in the small-angle diffusion approximation (Rossi, 1952). We have used instead the following simple interpolation procedure:

(1) The pathlength s_B reached when the particle crosses the boundary $z = 0$ is taken to be

$$s_B = s_n + \frac{z_n}{z_n - z_{n+1}} (s_{n+1} - s_n) . \tag{38}$$

This would be strictly correct if the propagation within the nth step were rectilinear.

(2) If ω is the multiple scattering deflection in the nth step, and ω_B the corresponding deflection in the part of the step in which the pathlength is increased from s_n to s_B, we let

$$\cos \omega_B = 1 - (1 - \cos \omega) + \left(\frac{s_B - s_n}{s_{n+1} - s_n} \right) . \tag{39}$$

This relation, for small pathlength intervals $s_{n+1} - s_n$, would be exact if $\cos \omega$ and $\cos \omega_B$ were replaced by their mean values, and is also correct in the limiting $s_B = s_n$ and $s_B = s_{n+1}$. A small error arises

from the assumption, implicit in Eq. (39), that the obliquity cosine is a monotone increasing function of the pathlength, so that the possibility of an S-shaped trajectory within the step, for example, is disregarded.

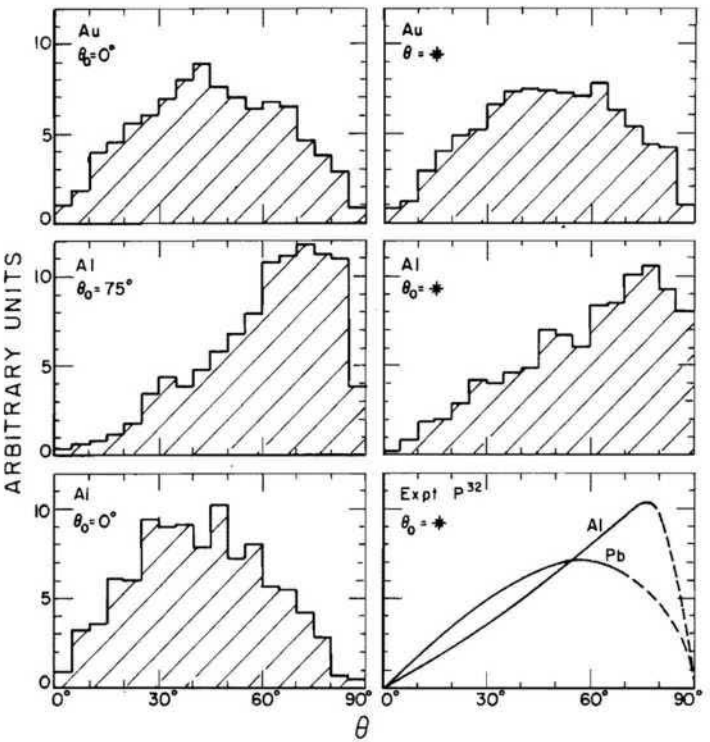

FIG. 4. Angular distribution of electrons reflected from a semiinfinite medium. The histograms represent Monte Carlo results for an incident energy of 0.5 Mev, obtained under the following conditions:

Medium	Direction of incidence	Number of histories	Monte Carlo model
Aluminum	0°	10,000	I, PLM (16/8, 48), EC, AGS, DL
Aluminum	75°	3,000	I, PLM (16/8, 48), EC, AGS, DL
Aluminum	Isotropic	3,000	I, PLM (16/8, 48), EC, AGS, DL
Gold	0°	5,000	I, PL (32, 96), EC, AGS, DL
Gold	Isotropic	5,000	I, PL (32, 96), EC, AGS, DL

The curves in the lower right-hand panel are from an experiment of Buys (1960) with an isotropic P^{32} beta ray source (maximum energy 1.7 Mev). Asterisk (*) indicates isotropic source.

(3) The deflection ω_B is inserted in Eq. (9) in place of ω, to obtain the direction of emergence θ_B.

Figure 4 shows angular histograms for electrons reflected from semiinfinite aluminum and gold media. To be consistent with our convention for describing histories, the angle θ should be taken between the direction of motion and the positive z-axis, and should thus lie between 90° and 180°. In fig. 4, we have instead taken it with respect to the negative z-axis, so that the angles of reflection range from $\theta = 0°$ (perpendicular to boundary) to $\theta = 90°$ (grazing). For perpendicular incidence, the angular distributions are diffuse and can be approximated by the function $\cos\theta \sin\theta\, d\theta$, i.e., by a cosine law, indicating that the electrons are reflected after so many collisions that they have "forgotten" their initial direction (a cosine-law for the emerging current corresponds to an isotropic flux near the boundary).

For isotropic incidence, electrons reflected from gold have a distribution not very different from a cosine-law but shifted slightly toward larger angles, whereas electrons reflected from aluminum emerge preferentially at very oblique angles. This can be understood qualitatively by a simple picture in which the reflected current is considered to consist of two components: the first the result of electrons incident more or less perpendicularly and reflected "diffusely," and the second the result of electrons incident obliquely which in turn are likely to emerge obliquely after few steps of the condensed random walk. For aluminum, the probability of diffuse backscattering is relatively small so that the obliquely reflected component dominates the angular distribution. This is not the case for gold, with its higher atomic number, in which diffuse backscattering has a much higher probability. Essentially the same argument has already been put forward by Seliger (1952) in the analysis of his experimental results, and is here confirmed by the Monte Carlo results. Further confirmation is provided by the experimental angular distributions, also shown in Fig. 4, obtained by Buys (1960) with isotropic beta-ray sources.

4. *Energy Spectrum of Reflected Electrons*

Figures 5 and 6 show energy spectra of electrons reflected from a semiinfinite aluminum medium. They were obtained by a Monte Carlo scheme of Class I (assuming the continuous-slowing-down approximation) and a subsequent correction to take into account energy loss fluctuations. The histograms labeled "b" and "a" represent the spectra obtained before and after application of this correction. The interval spacing of the histograms is logarithmic on an energy scale, and uniform

in respect to the "lethargy" variable

$$u = m \log_2 (E_0/E) \tag{40}$$

that can also be interpreted as the number of steps (with energy reduction factor $k = 2^{-1/m}$) that are taken before the electron emerges from the medium. As expected, more steps are required on the average when the direction of incidence is perpendicular than when it is isotropic. In the latter case, one can clearly distinguish two components of the spectrum consisting of electrons emerging either after many or after few steps. This is the analog of the division of the angular distribution into a diffuse and oblique component discussed in the preceding subsection.

In the continuous-slowing-down approximation one obtains essentially a pathlength distribution $L(s)$ of the reflected electrons. In lowest approximation, the corresponding energy spectrum is

$$Y^{(0)}(E) = L[s(E)] \left| \frac{dE}{ds} \right|^{-1}. \tag{41}$$

Energy loss fluctuations can be treated, in the next approximation, by folding the pathlength distribution into an energy loss distribution,

$$Y^{(1)}(E) = \int_0^{r_0} L(s)\, W_I(E_0 - E;\, E_0,\, s)\, ds \tag{42}$$

where $W_I(\Delta E, E_0, s)\, d(\Delta E)$ is the probability that an electron with initial energy E_0 will have an energy loss between Δ and $\Delta E + d(\Delta E)$ after traveling a pathlength s. Two small errors are made in this approximation. One disregards the correlation of the energy loss distribution with the pathlength distribution $L(s)$, and one evaluates W_I as if the medium were unbounded. Fully worked-out theoretical energy loss distributions are available only for the case $\Delta E \ll E_0$. They can be extended, however, to the case of large E, which is important in the present application, through a Monte Carlo calculation according to a scheme of Class I, the condensed history specification being limited to the pathlength and energy variables. The energy loss in each step is sampled from the appropriate theoretical distribution, and the corresponding loss for long pathlengths is obtained by summation. By sampling in this manner one derives a correction matrix which is applied to the spectral histogram and converts it into a corrected histogram that takes into account energy loss fluctuations. Such a correction matrix depends only on the nature of the medium and on the pathlength intervals but not on the boundary conditions, and can be used for the correction of diverse spectra.

In a quick survey of the energy-loss fluctuation effect, we have evaluated the correction matrix with the use of the Landau energy loss distribution [Eq. (A17) of the appendix] instead of the more correct and complicated distribution of Blunck and Leisegang (1950). Figures 5

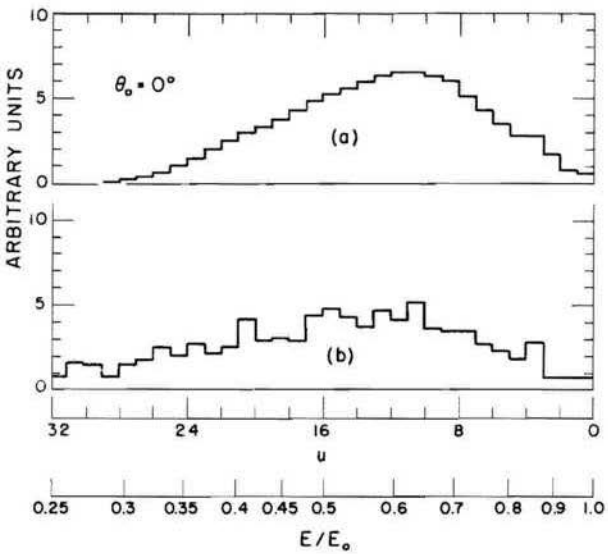

FIG. 5. Energy spectrum of electrons reflected from a semiinfinite aluminum medium. Source energy 0.5 Mev, perpendicular incidence. Histogram (b) represents results from 10,000 histories generated according to Model {I, PLM (16/8, 48), EC, AGS, DL}. Histogram (a) is the modified energy spectrum obtained from (b) by an approximate correction for energy loss fluctuations. Lethargy variable $u = 16 \log_2 (E_0/E)$.

TABLE XIV

TRANSMISSION OF ELECTRONS THROUGH ALUMINUM FOILS.[a]

a. Perpendicular incidence.

	z/r_0			
E_0, Mev	0.2	0.3	0.4	0.5
2.0	0.962 ± 0.006	0.847 ± 0.011	0.689 ± 0.015	0.469 ± 0.016
1.0	0.925 ± 0.008	0.785 ± 0.013	0.608 ± 0.015	0.373 ± 0.015
0.5	0.890 ± 0.010	0.751 ± 0.013	0.559 ± 0.016	0.361 ± 0.015
0.25	0.894 ± 0.010	0.738 ± 0.014	0.538 ± 0.016	0.306 ± 0.015
0.125	0.880 ± 0.010	0.731 ± 0.014	0.531 ± 0.016	0.321 ± 0.015

[a] Based on 1000 Monte Carlo histories for each source energy E_0, generated according to Model {I, PL (16, 96), EC, AM, DLT}.

b. Isotropic incidence.

	z/r_0			
E_0, Mev	0.2	0.3	0.4	0.5
2.0	0.635 ± 0.015	0.497 ± 0.016	0.339 ± 0.015	0.182 ± 0.012
1.0	0.585 ± 0.016	0.439 ± 0.016	0.298 ± 0.015	0.174 ± 0.012
0.5	0.590 ± 0.016	0.453 ± 0.016	0.306 ± 0.015	0.146 ± 0.011
0.25	0.577 ± 0.016	0.423 ± 0.016	0.268 ± 0.014	0.129 ± 0.011
0.125	0.558 ± 0.016	0.420 ± 0.016	0.264 ± 0.014	0.123 ± 0.011

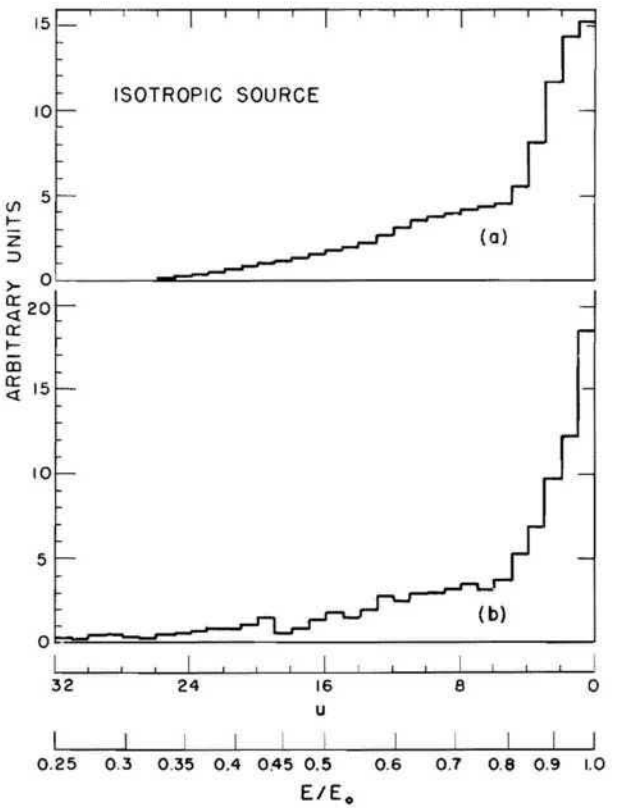

FIG. 6. Energy spectrum of electrons reflected from a semiinfinite aluminum medium. Source energy 0.5 Mev, isotropic source. Based on 3000 histories generated and utilized as described in caption of Fig. 5.

and 6 show that the correction is small for reflected electrons and results in a slight shift of the spectral distribution toward higher energies.

B. Transmission and Penetration of Electrons and Positrons

1. *Transmission Coefficients*

Table XIV contains Monte Carlo results on the transmission of electrons through aluminum foils, for various source energies and geometries. The outstanding feature is that the transmission coefficients, when expressed as functions of z/r_0, are insensitive to the value of the source energy (below 1 Mev), which is a confirmation of theoretical expectations.

In Fig. 7, Monte Carlo results are compared with recent precise experimental determinations of the transmission of electrons through aluminum and gold foils by Agu *et al.* (1958b). For small and intermediate foil thicknesses there is good agreement. For large thicknesses,

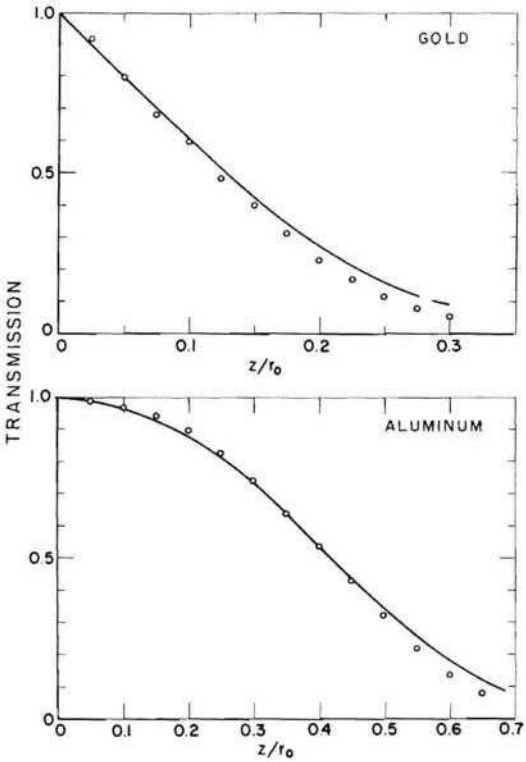

Fig. 7. Comparison of calculated and measured electron transmission through foils. The curves represent experimental results of Agu *et al.* (1958b) averaged for source energies between 0.25 and 0.75 Mev. The circles (o) represent Monte Carlo calculations for a source energy of 0.5 Mev, based on 5000 histories in aluminum, Model {I, PL(16.48), EC, AGS, DL}, and 2000 histories in gold, Model {I, PL (32,96), EC, AGS, DL}.

when the transmission becomes smaller than 30%, the experimental curves lie somewhat above the Monte Carlo results, which is due to the use of the continuous-slowing-down approximation. The disregard of energy-loss fluctuations of course greatly simplifies the computations, and Fig. 7 gives an indication of the rather wide limits within which this simplification will give reasonable results.

Just as positrons are backscattered less than electrons, their transmission is greater. Typical positron-electron transmission ratios are shown in Fig. 8. For gold they are in good agreement with experimental

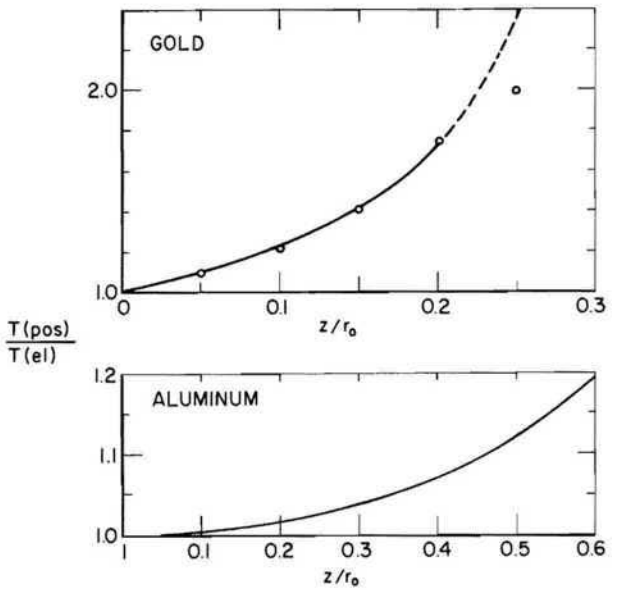

FIG. 8. Ratio of positron transmission to electron transmission through foils, for perpendicular incidence and a source energy of 0.5 Mev. Based on electron and positron histories generated as indicated in caption of Fig. 7. Circles (o) represent experimental results of Seliger (1955) with a 0.390-Mev source (r_0 = 0.245 gm/cm² gold for electrons, 0.240 gm/cm² gold for positrons).

results of Seliger (1955). Seliger's ratios for aluminum are greater than unity at 0.960 Mev but smaller than unity at energies below 0.336 Mev, so that a comparison with the calculated results at 0.5 Mev cannot readily be made.

The calculated ratios in Fig. 8 are actually somewhat too high because the positron transmission should be slightly reduced to take into account the possibility of annihilation in flight. From the theory of Bethe (1935) it can be estimated that the positron transmission for gold, for

the conditions of Fig. 8, should be reduced by approximately one per cent.

TABLE XV

DEPENDENCE OF CALCULATED ELECTRON TRANSMISSION ON MODEL OF CONDENSED RANDOM WALK.[a]

z/r_0	[b]	[c]	[d]	[e]
0.1	0.985 ± 0.004	0.977 ± 0.005	0.983 ± 0.004	0.984 ± 0.004
0.2	0.920 ± 0.027	0.914 ± 0.028	0.925 ± 0.026	0.919 ± 0.027
0.3	0.795 ± 0.040	0.780 ± 0.042	0.785 ± 0.041	0.787 ± 0.041
0.4	0.609 ± 0.049	0.584 ± 0.049	0.608 ± 0.049	0.609 ± 0.049
0.5	0.389 ± 0.049	0.366 ± 0.048	0.373 ± 0.048	0.376 ± 0.049

[a] For 1-Mev electrons incident perpendicularly on an aluminum foil. Based on 1000 histories.

[b] Model {I, PL(16,96), EC, AGS(Mott), DLT}.

[c] Model {I, PL(16, 96), EC, AGS (Rutherford), DLT}.

[d] Model {I, PL(16, 96), EC, AM (Molière), DLT (long. and transv.)}.

[e] Model {I, PL(16,96), EC, AM (Molière), DL (long. only)}.

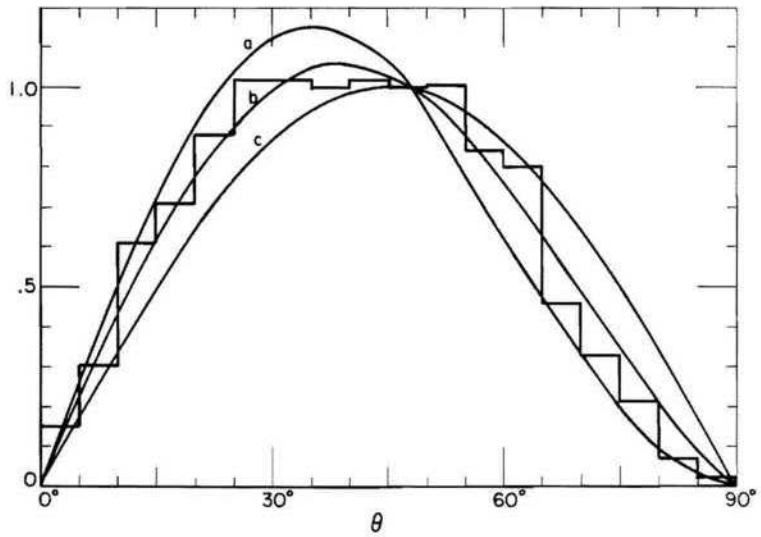

FIG. 9. Angular distribution of electrons transmitted through an aluminum foil 0.113 gm/cm² thick. Perpendicular incidence source energy 0.5 Mev. The histogram was obtained from the analysis of 4000 histories generated according to Model {I, PLM(16/8, 48), EC, AGS, DL}. Curves (a), (b) and (c) represent the functions $3\cos^2\theta\sin\theta$, $1.445(0.717\cos\theta + \cos^2\theta)\sin\theta$, and $2\cos\theta\sin\theta$, respectively.

Table XV illustrates the dependence of the calculated transmission coefficients on the multiple-scattering angular distribution used in the Monte Carlo scheme. The differences are much less than in the comparison of backscattering in Table XII, and are hardly significant statistically. Again, the neglect of transverse spatial multiple-scattering deflections appears to be of no consequence.

2. *Angular Distribution and Energy Spectrum of Transmitted Electrons*

The direction of transmitted electrons as they cross the foil boundary was determined by the same kind of interpolation procedure used in the backscattering problem. Figure 9 shows a typical angular distribution, for 0.5-Mev electrons incident on a foil of thickness $z/r_0 = 0.5$. The distribution appears to lie between a cosine-law and a cosine-

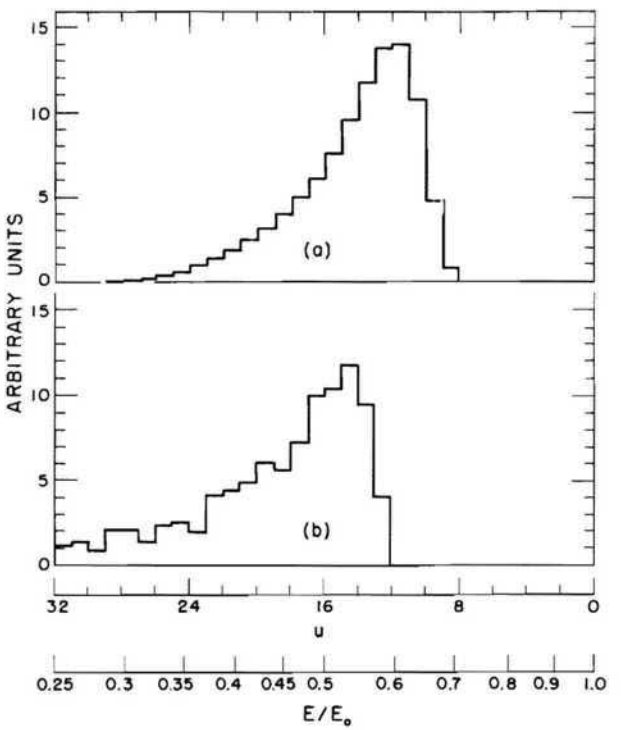

FIG. 10. Energy spectrum of electrons transmitted through an aluminum foil 0.113 gm/cm² thick. Perpendicular incidence, source energy 0.5 Mev. Histogram (*b*) is based on 4000 histories generated according to Model {I, PLM (16/8, 48), EC, AGS, DL}. Histogram (*a*) is the modified energy spectrum obtained from (*b*) through an approximate correction for energy loss fluctuations. Lethargy variable $u = 16 \log_2(E_0/E)$.

square law, and is actually described fairly well by the function $(0.717 \cos\theta + \cos^2\theta)\sin\theta$, which is the leading term of a result derived by Bethe *et al.* (1938) in a treatment disregarding energy loss.

Figure 10 shows an energy spectrum of transmitted electrons, for the same conditions as in Fig. 9. Two histograms are shown, one obtained in the continuous-slowing-down approximation and the other corrected for energy loss fluctuations. The correction is similar to that made in the backscattering problem, but the shift of the corrected spectrum toward higher energies is much more pronounced.

Hebbard and Wilson (1955) have calculated the transmission of electrons through aluminum and gold foils of moderate thickness, taking energy loss fluctuations into account from the beginning rather than by a subsequent correction. Figure 11 shows their results for the

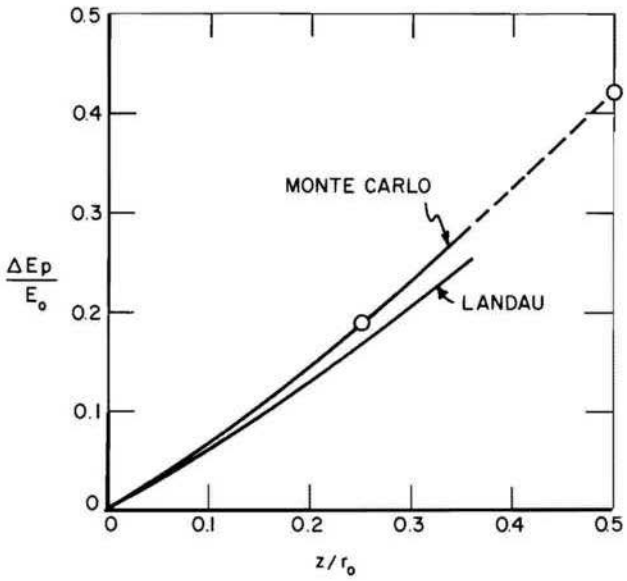

FIG. 11. Ratio of most probable energy loss ΔE_p, to the incident energy E_0, for 1-Mev electrons traversing an aluminum foil (Hebbard and Wilson, 1955). The Hebbard-Wilson curve labeled "Monte Carlo" is derived from 1000 histories generated according to Model {I, PU(Δs = 5.26 mg/cm^2), EI, AM, DL}. The circles (o) represent Monte Carlo results derived from a calculation similar to that described in Fig. 10.

most probable energy loss as a function of the foil thickness. Also shown are two Monte Carlo results derived from the data in Fig. 10 and similar data, which are in good agreement with the Hebbard-Wilson curve or its extrapolation, which indicates that our correction procedure has

some validity. The deviation of the Hebbard-Wilson curve from the corresponding curve predicted by the energy loss theory of Landau exhibits the effect of multiple scattering detours.

3. *Emergence of Electrons from the Interior of a Medium*

We consider a plane isotropic source of electrons at $z = 0$, sandwiched by two foils of thickness z, and want to know the electron current that emerges through the exterior surfaces of the two foils. Such problems arise, for example, when foils are bombarded with neutrons and the induced radioactivity of the foils is measured by counting the number of beta particles emitted. We shall compare Monte Carlo results with a calculation by Meister (1958) based on the diffusion theory of Bethe *et al.* (1938). He assumed that after leaving the source the electrons travel a distance of s' in a straight line until their energy has fallen to some intermediate value E', and that thereafter their propagation can be described by a diffusion equation. The energy E' is so adjusted that the mean square displacement in the z-direction, as function of the electron energy, agrees as closely as possible with the result of an exact transport calculation.

In the age-diffusion approximation for electrons, continuous-slowing-down is assumed, and the flux $F_0(z, s)$, integrated over all electron directions, is calculated by solving the diffusion equation

$$\frac{\partial F_0}{\partial \tau} = \frac{\partial^2 F_0}{\partial z^2} \tag{43}$$

with the appropriate boundary conditions. The "age"

$$\tau = \int_{s'}^{s} \frac{ds''}{3G_1(s'')} = \int_{E}^{E'} \frac{dE''}{3G_1[s(E'')]} \left| \frac{dE}{ds} \right|^{-1} \tag{44}$$

is related to the scattering cross section through the function $G_1(s)$ previously defined in Eq. (16). The reciprocal of G_1 is called the transport mean free path. The associated current $F_1(z, s)$ is obtained from the flux by differentiation,

$$F_1(z, s) = -\frac{1}{3G_1(s)} \frac{\partial F_0}{\partial z} . \tag{45}$$

In order for the age-diffusion approximation to be applicable, the following condition, among others, must be satisfied,

$$\frac{d}{ds} [1/G_1(s)] \ll 1 . \tag{46}$$

In the problem of a plane isotropic source sandwiched by two foils, the boundary conditions are that no electron current is incident on the foils from the outside. The current emerging from the foils, when normalized to unit source strength, can be interpreted as a transmission coefficient. Meister investigated this transmission coefficient by calculation and experimentally for a source emitting 0.312-Mev electrons (conversion electrons from an isomer of In^{115} produced by neutron irradiation). He found good agreement for gold and indium foils, but a discrepancy for aluminum, which he ascribed to the fact that Eq. (46) is satisfied only for media with atomic number $Z > 30$.

Monte Carlo calculations for aluminum are compared in Fig. 12 with

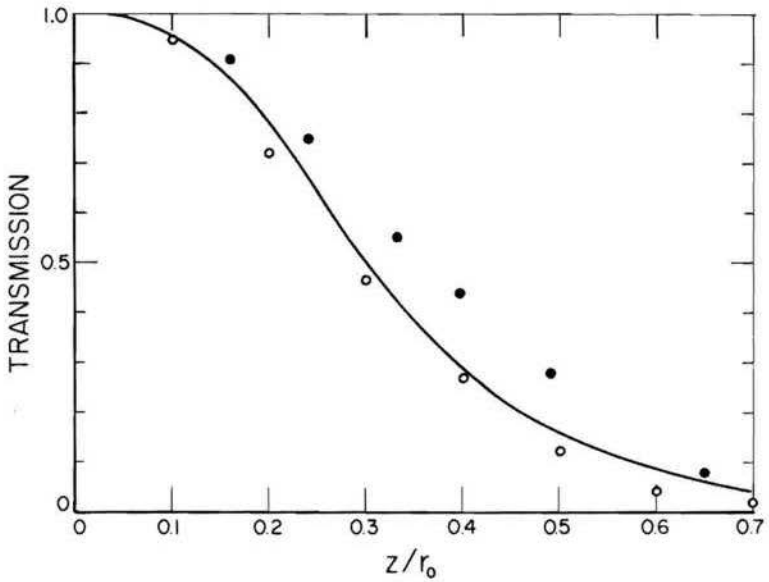

FIG. 12. Emergence of electrons from the interior of an aluminum medium. A plane isotropic source, emitting 0.312 Mev electrons (with mean range $r_0 = 0.114$ gm/cm^2) is assumed to be sandwiched between two layers of aluminum of thickness z. The curve, derived from an age-diffusion calculation, and the solid points (o) (experimental) are from a paper by Meister (1958). The open circles (o) represent Monte Carlo results based on 4000 histories generated according to Model {I, PL(16,96), EC, AGS, DL}.

Meister's results. Surprisingly, they are in fair agreement with his age-diffusion calculation, but deviate even more than the latter from the experimental points. The fractional deviation increases with increasing foil thickness, except for the last experimental point at $z/r_0 = 0.65$. The possibility suggests itself that the deviation may be because of the

neglect of energy loss fluctuations in both calculations. However, it is difficult to understand why the effect of these fluctuations is much greater in the present problem than for the transmission data described in Fig. 7.

4. *Influence of Bremsstrahlung on the Penetration of Very Fast Electrons*

The penetration of charged particles at high energies, where bremsstrahlung plays a paramount role, was first calculated by the Monte Carlo method by Wilson (1950, 1951). His work was concerned with the development of electron- and photon-initiated showers in lead at energies up to 300 Mev, and with the range and straggling of electrons in lead at energies up to 1000 Mev. In first approximation, he considered only energy losses by bremsstrahlung and ionization, and assumed the propagation of the radiation to be rectilinear. In a second approximation, he estimated the shortening of the electron mean range due to multiple-scattering detours. The calculations were done by hand, the

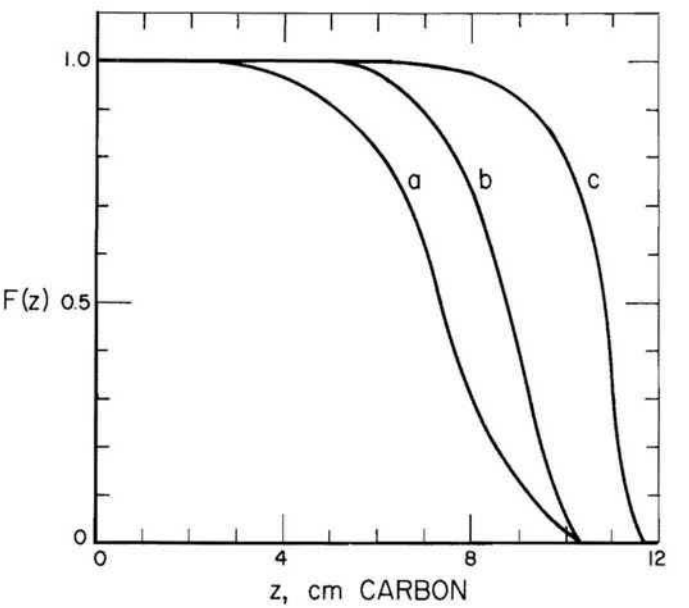

FIG. 13. Integral range-straggling distribution for 30-Mev electrons in carbon (Leiss *et al.*, 1957). $F(z)$ is the fraction of the incident electrons that penetrate at least to depth z. Curve (*c*) takes into account only fluctuations of ionization losses, curve (*b*) in addition includes the effect of multiple scattering detours, and the final result, curve (*a*), also include effects of bremsstrahlung losses. Curve (*a*) was obtained from the analysis of 1000 histories generated according to Model {I, PU(1/4 cm carbon), EIB, AG, DL}.

random sampling being done with the use of a physical device (wheel of chance) rather than with the use of random numbers. The method involved the grouping of collisions, the step size of the condensed random walk being 0.2 of a radiation length (1.2 g/cm^2 of lead).

More elaborate calculations with a computer were done by Leiss *et al.* (1957) who determined the integral range straggling distribution $F(z)$, i.e., the fraction of the incident electron beam that penetrates at least to depth z, for a carbon medium and energies up to 55 Mev. They used a Class-I scheme with a uniform step size of 1/4 cm, compounding the energy loss per step from an ionization loss, sampled from the Landau distribution, and a bremsstrahlung loss, sampled from a distribution derived by Eyges (1949). The latter, for the conditions of the calculation of Leiss *et al.*, takes the form

$$W_B(\epsilon_B)\, d\epsilon_B = 0.01278(1 - \epsilon_B)^{1/4}[\log (1 - \epsilon_B)^{-1}]^{-0.9874}\, d\epsilon_B\,, \qquad (47)$$

where ϵ_B is the fractional energy loss as a result of bremsstrahlung. In a history generated in this fashion, very large energy losses are mainly due to bremsstrahlung. For example, the probability that a 20-Mev electron will, in a pathlength of 1/4 cm of carbon, lose and energy greater than 3 Mev is about 0.2% for ionization but 1.7% for bremsstrahlung, whereas the probability of a loss greater than 0.5 Mev is practically 100% for ionization, but only 3.6% for bremsstrahlung.

Figure 13 shows the integral range straggling distribution of Leiss *et al.* for 30-Mev electrons. Auxiliary curves are also shown which indicate the relative contributions to the shape of the distribution due to ionization loss fluctuations, bremsstrahlung loss fluctuations, and multiple-scattering detours. The corresponding mean range, in the continuous-slowing-down approximation, is 10 cm of carbon.

C. Energy Dissipation by Electrons in Bounded and Unbounded Media

In radiological applications it is of considerable interest to know the spatial pattern of energy dissipation by diffusing electrons. We have obtained some Monte Carlo results for plane sources in infinite and semiinfinite media, in the continuous-slowing-down approximation. The entire electron energy must be dissipated at points no farther from the source plane than the initial electron range r_0. Accordingly, the region $-r_0 \leqslant z \leqslant r_0$ was divided into forty equal subregions. When a step of a condensed history fell entirely within one of these subregions, the energy $E_n - E_{n+1}$ was assumed to be dissipated there. When the step straddled the boundary of two subregions, this energy was assumed to

be deposited in both, in proportion to the pathlength in each. The step sizes were small enough so that only one boundary between subregions could be straddled at one time, and even this happened rarely. The same set of histories was used for the evaluation of energy deposition in infinite and semiinfinite media, which constituted another application of the technique of correlated sampling.

A very accurate calculation of energy deposition in infinite media has been carried out by Spencer (1955, 1959) who computed the spatial moments of the distribution function from a transport equation that was exact except for the use of the continuous-slowing-down approximation, and constructed the distribution from a knowledge of its moments and its asymptotic behavior for deep penetration. Figure 14, pertaining to a plane perpendicular source, shows a Monte Carlo histogram that is in good agreement with Spencer's result. Figure 15 contains a similar

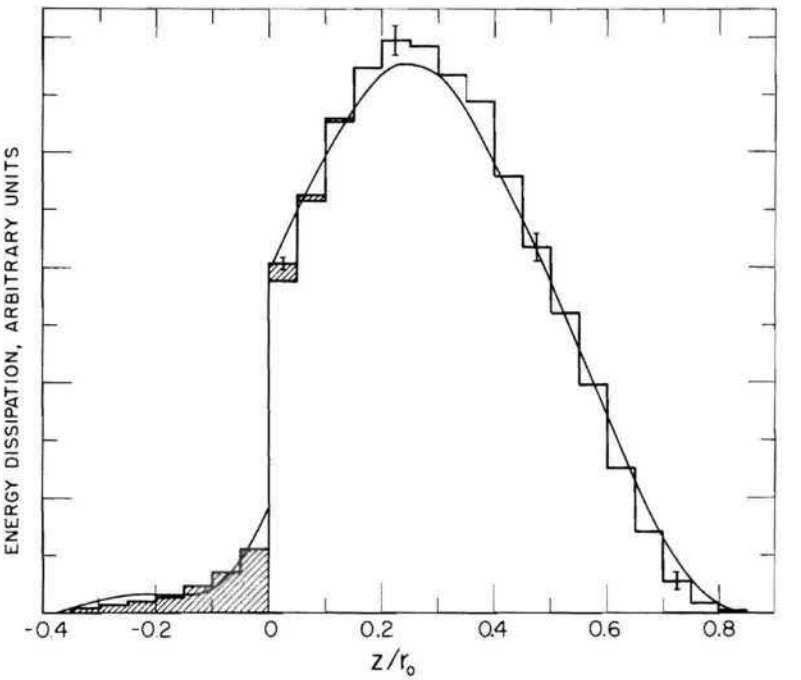

FIG. 14. Energy dissipation by electrons in aluminum. Electrons are assumed to originate from a 1-Mev plane perpendicular source at $z = 0$. The curve represents a calculation, by the moment-method, of Spencer (1959). The histogram is derived from 5000 histories generated according to Model {I, PL(16,48), EC, AGS, DL}. The shaded portions of the histogram indicate the reduction of energy dissipation, resulting from the escape of electrons, that would occur if the medium were semiinfinite ($0 < z < \infty$) rather than infinite.

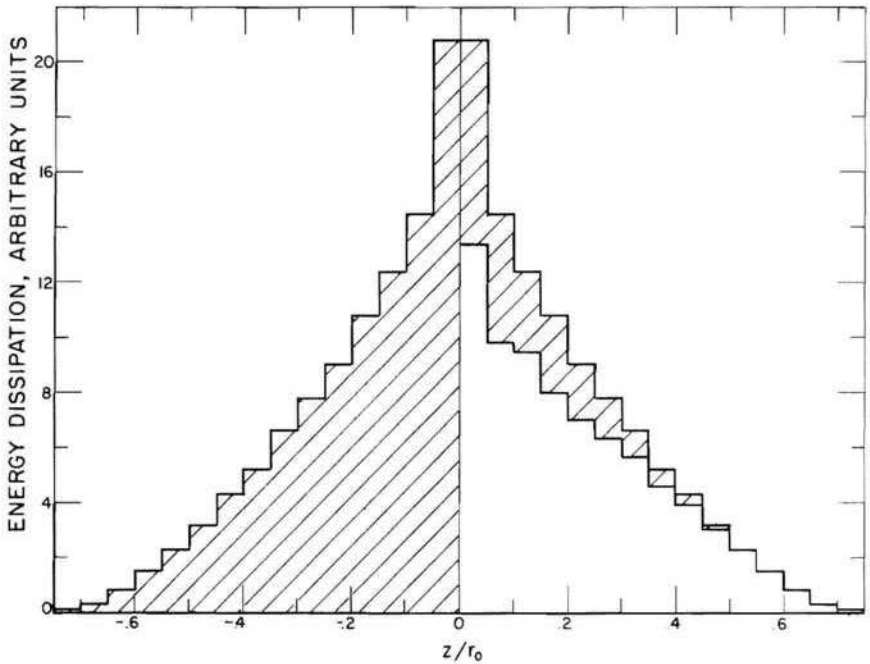

FIG. 15. Energy dissipation by electrons in aluminum. Based on 3000 histories generated as described in caption of Fig. 14, but for plane isotropic source at $z = 0$. Again, shaded portions of histogram indicate the reduction of energy dissipation due to electron escape from a semiinfinite medium.

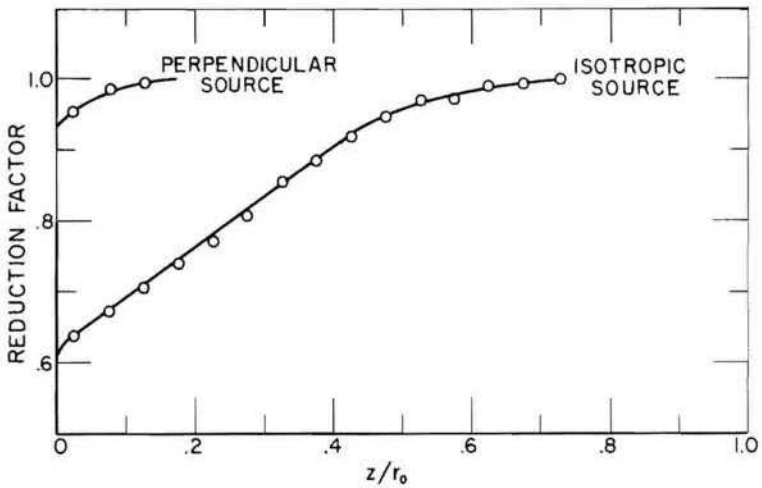

FIG. 16. Reduction of energy dissipation near the boundary of a semiinfinite medium. Based on Monte Carlo results for a 1-Mev source in aluminum shown in Figs. 14 and 15.

Monte Carlo histogram for a plane isotropic source. In both figures the histograms represent energy dissipation in an infinite medium, and their shaded portions indicate the reduction of energy dissipation that would occur if the medium were semiinfinite, because of the leakage of electrons through the boundary $z = 0$. The determination of such a boundary effect is a very trivial task for the Monte Carlo method but cannot be done by the moment-method. In Fig. 16, the boundary effect is plotted as a function of the distance from the boundary. The reduction of energy dissipation is seen to be small for the perpendicular source, whereas it is considerable and extends to great distances for the isotropic source. The latter situation is realized when a medium is covered with a thin layer of radioactive material emitting beta particles.

D. Slowing-Down Spectrum and Pathlength Straggling of Electrons

The problems discussed in this section, involving the energy and pathlength variables only, were first treated by Schneider and Cormack (1959) by a Monte Carlo scheme of Class II. Their computations were done by hand and were thus limited to a few hundred histories. The numerical results presented here are based on similar but more extensive machine calculations.

The first problem concerns the *slowing-down spectrum* which may be defined as the energy spectrum that is established as the result of multiple Coulomb scattering in a medium in which an electron source is distributed uniformly.

If the energy loss of the diffusing electrons were continuous, the slowing-down spectrum would be inversely proportional to the electron stopping power, which can be seen by the following argument. To each electron we may assign an age t, which is equal to the time it has spent in the medium since leaving the source. Under steady-state conditions, the number of electrons with ages between t and $t + dt$ is proportional to dt, but does not depend on t itself. The number of electrons with pathlengths between s and $s + ds$ is proportional to $dt/ds\, ds = ds/v$, and the flux of electrons with energies between E and $E + dE$ is

$$F(E)\, dE = Sv\left(\frac{ds}{v}\right) = S\frac{dE}{\left|\frac{dE}{ds}\right|}, \tag{48}$$

where S is the source strength.

We recall that in Monte Carlo schemes of Class II the cumulative effect of collisions with small fractional energy losses $\epsilon < \epsilon_c$ is assumed

to result in a continuous slowing down of the electrons, which is occasionally interrupted by catastrophic collisions with $\epsilon > \epsilon_c$ as the result of which the electron may jump across certain energy intervals (see Fig. 2). The expression for the slowing-down spectrum, in this schematization, must be modified to read

$$F(E)\,dE = SP(E, \epsilon_c) \frac{dE}{\left| \frac{dE}{ds} \right|_{\epsilon_c}}, \tag{49}$$

where $P(E, \epsilon_c)$ is the probability that an electron will have an energy E at some stage of its history, and where $| dE/ds |_{\epsilon_c}$ is the stopping power evaluated with a cutoff ϵ_c. Both $P(E, \epsilon_c)$ and $| dE/ds |_{\epsilon_c}$ decreases as ϵ_c decreases. The applicability of Eq. (49) depends on the fact that their ratio tends toward a limiting value for small ϵ_c for which the Class-II schematization is still valid. (If ϵ_c were allowed to go to zero, there would be no more continuous-slowing-down.) $P(E, \epsilon_c)$ can easily be determined through inspection of a set of sampled Class-II histories.

TABLE XVI

SLOWING-DOWN SPECTRUM OF ELECTRONS IN ALUMINUM[a].

E (Mev)	$1 \left\lvert \frac{dE}{ds} \right\rvert$[b]	Spencer-Fano[c] theory	Monte Carlo[d]		
			$\epsilon_c = 0.1$	$\epsilon_c = 0.03$	$\epsilon_c = 0.01$
0.6450	0.647	(0.7025)	(0.710)	(0.748)	(0.750)
0.6400	0.646	(0.698)	0.703	0.737	0.740
0.6200	0.644	(0.681)	0.689	0.700	0.700
0.6000	0.640	(0.668)	0.678	0.674	0.690
0.5827	0.637	0.6581	0.667	0.661	0.657
0.5500	0.631	(0.641)	0.652	0.647	0.642
0.5191	0.625	0.6284	0.637	0.637	0.631
0.4625	0.610	0.6055	0.609	0.607	0.610
0.3270	0.555	0.5450	0.552	0.553	0.557
0.2312	0.487	0.4840	0.492	0.488	0.475
0.1635	0.414	0.4237	0.424	0.426	0.441
0.1156	0.342	0.3687	0.364	0.374	0.371
0.08176	0.275	0.3233	0.322	0.317	0.323
0.05779	0.219	0.2893	0.290	0.284	0.280

[a] The spectrum is given as differential track length and has dimensions g cm^{-2} Mev^{-1}. Source energy 0.6450 Mev. Values in parentheses are interpolated or extrapolated.

[b] Reciprocal of mean energy loss by ionization (evaluated with $\epsilon_c = 0.5$).

[c] As evaluated by McGinnies (1959).

[d] Based on 1000 Model-II histories for each value of ϵ_c.

The slowing-down spectrum has been studied by Spencer and Fano (1954) who developed a method for the accurate numerical integration of the appropriate transport equation. Table XVI gives a comparison of Monte Carlo results with a spectrum obtained by McGinnies (1959) according to the Spencer-Fano method. Both methods of computation give the same spectrum, to within the accuracy of the Monte Carlo results, and the latter are practically independent of the value of the cutoff parameter in the range ($0.01 \leqslant \epsilon_c \leqslant 0.1$), at all spectral energies except very close to the source energy. Actually the spectrum diverges at the source energy and rises very steeply in its vicinity. The values in the top line of Table XVI are extrapolations indicative of the spectrum near the source energy. Energy loss straggling is seen to increase the slowing-down spectrum at high spectral energies compared to the value in the continuous-slowing-down approximation (inverse of the stopping power). This is similar to the shift of the spectra of reflected and transmitted electrons in Figs. 5, 6, and 10 toward higher energies. At low energies, the correct slowing-down spectrum again exceeds the reciprocal of the stopping power, because of the appearance of secondary knock-on electrons. The ratio of the total to the primary flux is given in Table XVII. Again, the Monte Carlo results are insensitive to the value of ϵ_c and in agreement with the predictions of the Spencer-Fano theory. Finally, Table XVIII shows the frequency distribution of the number of secondary knock-on electrons.

Within the schematization of Class II, the effect of energy loss fluctuations on the distance traveled by electrons in the course of slowing down is twofold. On the one hand, the pathlength is increased compared to its value in the continuous-slowing-down approximation,

TABLE XVII

RATIO OF TOTAL TO PRIMARY ELECTRON FLUX IN ALUMINUM.[a]

E (Mev)	Spencer-Fano[b] theory	Monte Carlo[c] $\epsilon_c = 0.1$	Monte Carlo[c] $\epsilon_c = 0.03$	Monte Carlo[c] $\epsilon_c = 0.01$
0.2312	1.001	1.01	1.01	1.01
0.1635	1.031	1.03	1.04	1.05
0.1156	1.086	1.09	1.09	1.13
0.08176	1.180	1.20	1.18	1.21
0.05779	1.332	1.34	1.31	1.32

[a] Source energy 0.6450 Mev.

[b] Calculated by McGinnies (1959).

[c] Based on 1000 model-II histories for each value of ϵ_c.

TABLE XVIII

PRODUCTION OF SECONDARY ELECTRONS[a]

No. of secondary electrons	Monte Carlo[b]		
	$\epsilon_c = 0.1$	$\epsilon_c = 0.03$	$\epsilon_c = 0.01$
0	713	771	695
1	255	263	280
2	28	25	24
3	4	1	1

[a] Frequency with which a primary 0.6450-Mev electron gives rise to a cascade of 0, 1, 2, 3, ... secondary electrons with energies between 0.3225 Mev (the highest possible secondary energy) and 0.0578 Mev, in an aluminum medium.

[b] Based on the analysis of Model-II histories of 1000 primary electrons and their secondaries.

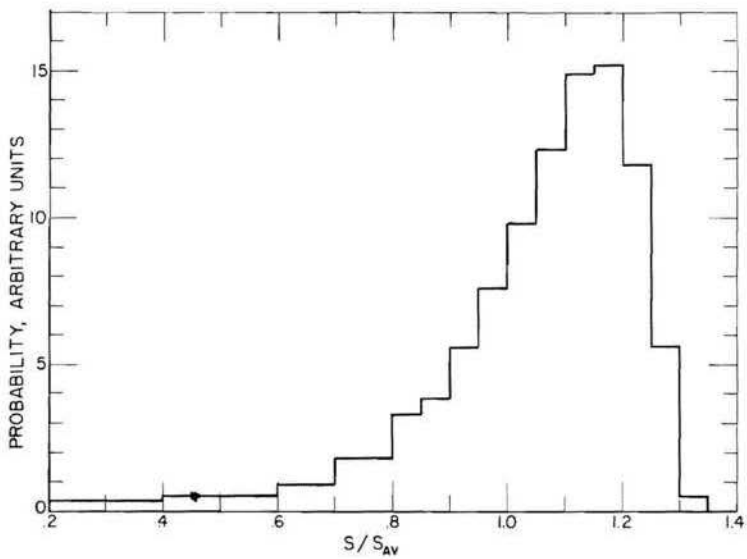

FIG. 17. Pathlength traveled by electrons in aluminum, in the course of slowing down from 0.5 to 0.25 Mev. The histogram was obtained from 7000 histories generated according to Model II with a cutoff $\epsilon_c = 0.01$. $s_{av} = 0.143$ gm/cm^2 is the mean pathlength calculated in the continuous-slowing-down approximation.

because of the energy transfer cutoff ϵ_c which reduces the mean energy loss per unit pathlength. On the other hand, the possibility of catastrophic collisions tends to reduce the pathlength required to reach a given energy. The interplay of the two effects leads to a pathlength

distribution determined by the statistical occurrence of catastrophic collisions. Figure 17 shows a typical distribution for electrons slowing down in aluminum from 0.5 Mev to 0.25 Mev. It is strongly skewed such that the most probable pathlength exceeds the mean pathlength.

The mean pathlength given by the Monte Carlo calculation exceeds the value obtained in the continuous-slowing-down approximation from the expression

$$\langle s \rangle_{\mathrm{av}} = \int_{E}^{E_0} \left| \frac{dE}{ds} \right|^{-1} dE , \tag{50}$$

with $| dE/ds |^{-1}$ evaluated as the reciprocal of the mean of $| dE/ds |$. As shown in Table XIX, this discrepancy is greatest for very short pathlengths, when the electrons have lost only little energy, and eventually vanishes when they have been slowed down to very low energies. The reason for the discrepancy appears to be that it would actually be more correct to use in Eq. (50) the mean value of the reciprocal $| dE/ds |^{-1}$. Such an average is not readily available from stopping power theory. It is plausible, however, that the energy loss fluctuations will make the mean value of the reciprocal greater than the reciprocal of the mean value of $| dE/ds |$. The bearing of this discrepancy on the use of the continuous-slowing-down approximation in transport calculations should be examined.

TABLE XIX

PATHLENGTH OF ELECTRONS[a]

E (Mev)	$\langle s \rangle_{\mathrm{av,MC}} / \langle s \rangle_{\mathrm{av}}$	
	Aluminum	Gold
0.4788	1.24	1.28
0.4585	1.18	1.23
0.4391	1.15	1.18
0.4204	1.12	1.15
0.4026	1.10	1.13
0.3536	1.08	1.09
0.2973	1.05	1.06
0.2500	1.03	1.04
0.1768	1.01	1.01
0.1250	1.01	1.00
0.0625	1.00	1.00

[a] Pathlength of electrons slowing down from an initial energy of 0.5 Mev to energy E. $\langle s \rangle_{\mathrm{av,MC}}$ is the average pathlength obtained from the analysis of 1000 Model-II histories and $\langle s \rangle_{\mathrm{av}}$ is the corresponding average calculated on the assumption of continuous-slowing-down. Statistical error of the Monte Carlo results is ~ 0.02.

E. Penetration of Protons

1. *Analysis of a Stopping Power Experiment*

Measurements of the penetration of protons through thick foils can be used to derive the value of the one parameter in the Bethe theory of stopping power that cannot yet be evaluated theoretically, namely, the mean ionization potential I (see Eqs. A9 and A12 of the appendix). We shall discuss Monte Carlo calculations pertinent to the analysis of a precise experiment by Mather and Segrè (1951) in which 340-Mev protons were incident on thick foils and the ionization due to transmitted photons was measured with an argon-filled ionization chamber.

If there were no multiple-scattering detours and energy loss fluctuations, the observed ionization as function of the foil thickness, $R(z)$, would vanish abruptly at a thickness z equal to the mean proton range r_0, and from this range one could readily determine I. Actually $R(z)$ has a rounded tail rather than an abrupt end, because of statistical fluctuations of the proton penetration, and a more elaborate analysis is needed. In Mather and Segrè's analysis, the statistical distribution of proton pathlengths (caused by energy loss fluctuations) was taken into account, but multiple-scattering detours were considered only insofar as they result in a *mean* difference between the depth of penetration and the pathlength. The shape of $R(z)$ thus derived was somewhat at variance with the observed shape. Mather and Segrè suggested that the value of I deduced by them was not likely to be affected by this discrepancy, and that nuclear interactions (disregarded in the analysis) were the most probable cause. The purpose of the Monte Carlo calculations was to find out to what extent a more thorough treatment of multiple scattering detours could remove the discrepancy, and to what extent this would alter the deduced value of I.

Expressed as a function of the proton flux $F(E, \theta, z)$, the observed ionization behind a foil of thickness z is

$$R(z) = \text{constant} \times \int_0^{E_0} dE \int_0^{\pi/2} \sin\theta \, d\theta F(E, \theta, z) \left| \frac{dE}{ds} \right|_A , \qquad (51)$$

where $| dE/ds |_A$ is the stopping power of the gas in the ionization chamber (argon). $R(z)$ was estimated from histories generated according to the Class-I′ scheme, with the multiple-scattering angular deflections selected from a Molière distribution, the pathlengths in each step from a Gaussian distribution. Actually the pathlength distribution for short steps is not exactly Gaussian but is slightly skewed (Lewis, 1952). The skewness is similar to that for electrons (see, e.g., Fig. 17) but is much smaller for protons and decreases rapidly with the mean pathlength.

The error caused by the neglect of the skewness is expected to be unimportant because $R(z)$ was calculated only for large z such that the cumulative pathlength of the protons emerging from the foil was long enough for the Gaussian approximation to be very good.

The histories were terminated when the proton energy fell below 2 Mev, which was permissible because the remaining distance of travel (e.g., 50 mg/cm² of lead) was very small compared to the accuracy with which the foil thickness is known and compared to the scale on which $R(z)$ is expressed. Each proton emerging from the foil was given a "score"

$$\frac{1}{\cos\theta}\left|\frac{dE}{ds}\right|_{A}, \tag{52}$$

where the factor $1/\cos\theta$ provided the conversion from current to flux, and $|\,dE/ds\,|_{A}$ (evaluated with $I = 197$ ev for argon) the conversion from flux to ionization. The average of many scores yielded an estimate of $R(z)$.

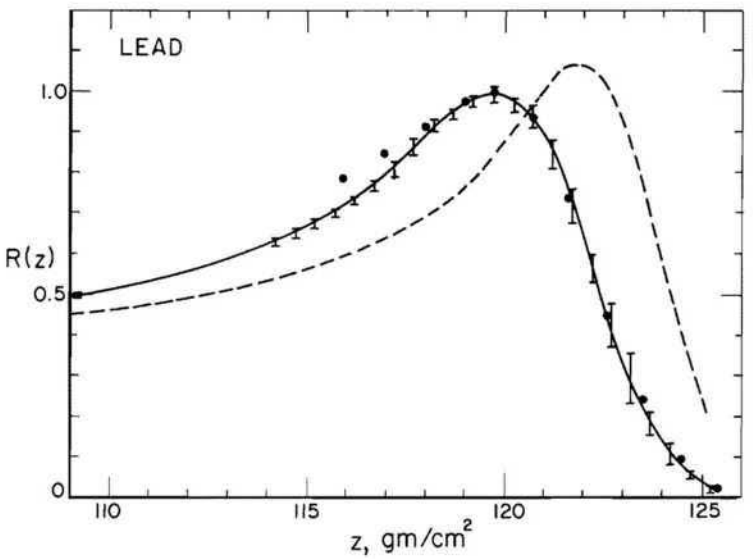

FIG. 18. Ionization $R(z)$ produced in an argon-filled ionization chamber by protons that have traversed a lead barrier of thickness z. Perpendicular incidences, source energy 338.5 Mev. The points (0) are from an experiment by Mather and Segrè (1951). The solid curve is obtained from 5000 histories generated according to Model I', with an assumed mean ionization potential $I = 802$ ev. The experimental and calculated values are both normalized so that the peak value of $R(z)$ is unity. The vertical bars represent limiting values of the Monte Carlo results, corresponding to different procedures for computing spatial displacements. The dotted curve is a Monte Carlo result obtained when multiple-scattering detours were disregarded.

In Figs. 18 and 19, calculated values of $R(z)$ for 338.5-Mev protons incident on lead and copper barriers are compared with the experimental results of Mather and Segrè (1951).[2] The adjustment of the

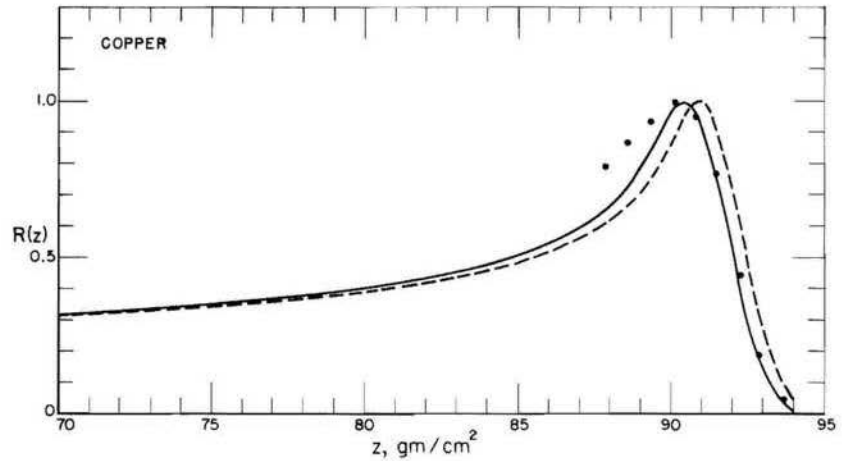

FIG. 19. Ionization $R(z)$, as described in caption of Fig. 18, but for a copper barrier. Assumed mean ionization potential in Monte Carlo calculation was $I = 305$ ev.

calculated data to the experimental data was based on the observation that the shape of $R(z)$ in the neighborhood of its peak remains practically unchanged when the assumed value of the mean excitation potential I is changed slightly, whereas the location of peak is shifted by an amount almost equal to the change of the mean range r_0. After some preliminary calculations with various I-values, a best fit in the immediate vicinity and to the right of the peak was obtained with $I = 802$ ev for lead and $I = 305$ ev for copper. These values are in good agreement with the values 792 ev, respectively, 304 ev, deduced by Mather and Segrè.

It should be noted that the uncertainty of the incident proton energy puts a limit on the accuracy with which one can determine I. For example, in lead at 340 Mev, $\Delta r_0/r_0 = 0.19\ \Delta I/I$ at constant E_0, and $\Delta r_0/r_0 = 1.6\ \Delta E_0/E_0$ at constant I, so that the same shift of the peak could be due to a 0.5% change of E_0 or a 5% change of I.

Inspection of Figs. 18 and 19 shows that to the left of the peak, the calculated results are slightly lower than the experimental results for lead, and significantly lower for copper. One reason for this discrepancy

[2] These data wese used, but not explicitly described, in the publication of Mather and Segrè, and were put at the author's disposal through the courtesy of Dr. R. L. Mather.

could be the inhomogeneity of the energy of the incident proton beam. However, Mather and Segrè estimated this inhomogeneity to be no greater than 0.5%, which might be enough to remove the discrepancy in lead but not in copper. Thus, the more elaborate analysis of multiple-scattering detours tends to confirm Mather and Segrè's original conclusion that nuclear interactions may have to be taken into account in order to obtain a complete understanding of the observed $R(z)$ curves, and the indications are that such effects would be more important for copper than for lead.

As has been indicated in Section III, A, 4, the z-displacement of the proton in each step of a condensed history was related to the pathlength by an approximate formula instead of being sampled from the appropriate distribution. The error incurred thereby becomes important for very deep penetration, so that it was investigated by three correlated calculations, in which the spatial displacements were evaluated as follows:

$$\text{Upper limit;} \qquad \Delta\zeta = \Delta s_n \tag{53}$$

$$\text{Usual interpolation formula;} \qquad \Delta\zeta = \Delta s_n \frac{1 + \cos\omega}{2} \tag{54}$$

$$\text{Approximate lower limit;} \qquad \Delta\zeta = \Delta s_n \cos\omega\,. \tag{55}$$

The solid curve in Fig. 18 was obtained with the use of Eq. (54) and the upper and lower ends of the vertical bars correspond to the results obtained with the use of Eqs. (53) and (55), respectively. Finally, Table XX shows that the value of $R(z)$ remains the same, within the limits of statistical accuracy, whether the step sizes for condensed histories are chosen uniform on a linear or a logarithmic energy scale.

TABLE XX

DEPENDENCE OF RELATIVE IONIZATION ON STEP-SIZE OF MODEL-I′ HISTORIES.[a]

z (gm/cm²)	$R(z)$	
	Uniform spacing[b]	Logarithmic spacing[c]
115.8	0.704 ± 0.004	0.689 ± 0.004
117.8	0.863 ± 0.008	0.843 ± 0.008
119.8	1.000 ± 0.012	1.000 ± 0.011
121.8	0.707 ± 0.014	0.720 ± 0.015
123.8	0.181 ± 0.010	0.189 ± 0.011

[a] 338.5 Mev protons in lead. 5000 histories consisting of 30 steps each.

[b] Approximately uniform step-size as indicated by Table IV(a).

[c] Step-size uniformly spaced on logarithmic energy scale as indicated by Table IV(*b*), with energy reduction factor $k = (2.0/338.5)^{1/30} = 0.8428$.

3. *Multiple-Scattering Detours*

We next consider in more detail the difference between pathlength and depth of penetration,

$$s - z = \int_0^s [1 - \cos \theta(s')]\, ds' \tag{56}$$

and compare Monte Carlo results with two theories.[3]

Bichsel and Uehling (1960) have put forward an approximate simple theory based on the assumption of the small-angle approximation and

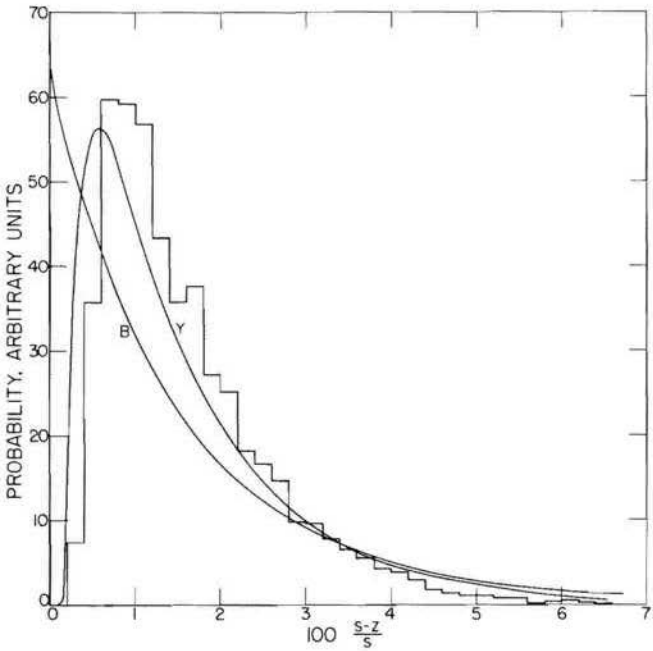

FIG. 20. Multiple-scattering detours. The pathlength distribution of protons slowed down in lead from 338.5 to 2.0 Mev is shown as a function of the percentage difference between the distance a traveled and the depth of penetration z. The histogram was obtained from 5000 histories generated according to Model I′, taking into account multiple-scattering deflections, but not energy loss fluctuations. Curve B represents the theory of Bichsel and Uehling (1960), and curve Y a modified version of the theory of Yang (1951).

[3] The variable θ represents the obliquity of the track with respect to the z-axis, and is a stochastic function of the pathlength s. It is analogous to the variable ω used in Section III, A which represents the obliquity of the track with respect to the φ-axis in a single step of the condensed random walk. θ is used here rather than ω because we are concerned with the difference between pathlength and depth of penetration for long tracks consisting of many steps.

of "smoothed-out" trajectories such that the reduced multiple-scattering deflection $\vartheta = \theta/\chi_c\sqrt{B}$ of the Molière theory remains constant along the path. Thus they replace the stochastic dependence of θ on s' by a deterministic dependence, and set

$$s - z = \frac{1}{2}\int_0^s \theta^2(s')\,ds' = \frac{1}{2}\vartheta^2 \int_0^s \chi_c{}^2 B\,ds' = \frac{1}{2}\vartheta^2 \int_E^{E_0} \chi_c{}^2 B \left|\frac{dE}{ds}\right|^{-1} dE' \qquad (57)$$

The distribution of $s - z$ then follows from the Molière distribution of ϑ. As can be seen from Fig. 20, the result is a distribution that is reasonable for large $s - z$ differences, but which—incorrectly—peaks at $z = s$.

Yang (1951) has solved this problem in the small-angle diffusion approximation, without taking into account energy loss, and obtained a distribution which he approximated as

$$\left.\begin{aligned} L(q)\,dq &= \frac{2}{(\pi q^3)^{1/2}}\,(e^{-1/q} - 3e^{-9/q})\,dq\,, \quad q \leqslant 2.0 \\ &= \frac{\pi}{4}\,e^{-\pi^2 q/16}\,dq\,, \qquad q > 2.0 \end{aligned}\right\} \qquad (58)$$

where

$$q = \frac{2(s - z)}{\langle s - z\rangle_{\mathrm{av}}}\,. \qquad (59)$$

This distribution includes all particles regardless of their direction at the end of the path.

The Monte Carlo calculations pertain to 340-Mev protons slowed down to 2 Mev in a lead medium, and yield an average pathlength difference

$$100\left\langle\frac{s - z}{s}\right\rangle_{\mathrm{av}} = 1.639 \pm 0.012$$

Inserting this result into Eq. (59) we have obtained a modified Yang distribution which, as shown in Fig. 20, is in good agreement with the Monte Carlo distribution, the peak being approximately at the right position. Thus it appears that the region of applicability of the Yang theory can be greatly extended when $\langle s - z\rangle_{\mathrm{av}}$ is obtained from an exact transport calculation, the form of his distribution remaining the same. Very similar findings have been made by Hebbard and Wilson (1955) for electron pathlength distributions.

ACKNOWLEDGMENTS

The author is indebted to Dr. L. V. Spencer for many helpful discussions, to Dr. R. L. Mather for placing unpublished data at his disposal, and to Dr. J. Coyne for the loan of a FORTRAN program to compute the Mott scattering cross section.

VI. Appendix: Single and Multiple Scattering Theories

The following symbols will be used:

m = mass of electron	E = kinetic energy
M = mass of proton	τ = kinetic energy in units of rest mass
e = charge of electron	N = number of atoms per cm^3
c = velocity of light	ρ = density of medium
v = velocity	Z = atomic number
$\beta = v/c$	A = atomic weight
p = momentum	

A. Energy Loss

1. *Scattering of Electrons by Electrons*

In this and the next subsection we follow the presentation of Rohrlich and Carlson (1954). The Møller cross section for the scattering of electrons by electrons is

$$\frac{d\sigma}{d\epsilon} = \frac{C}{E}\left\{\frac{1}{\epsilon^2} + \frac{1}{(1-\epsilon)^2} + \left(\frac{\tau}{\tau+1}\right)^2 - \frac{2\tau+1}{(\tau+1)^2}\frac{1}{\epsilon(1-\epsilon)}\right\}, \tag{A1}$$

where ϵ is the energy transfer in units of E, and

$$C = \frac{2\pi e^4}{mv^2}. \tag{A2}$$

With this energy transfer there is associated an angular deflection ω' (in the laboratory system) such that

$$\sin^2\omega' = \frac{4\epsilon}{\tau(1-2\epsilon)+\tau+4}. \tag{A3}$$

The probability distribution of energy transfers $\epsilon > \epsilon_c$ is

$$g(\epsilon;\epsilon_c)\,d\epsilon = \frac{\dfrac{d\sigma}{d\epsilon}}{\displaystyle\int_{\epsilon_c}^{1/2}\frac{d\sigma}{d\epsilon}}\,d\epsilon = \frac{\dfrac{d\sigma}{d\epsilon}}{\dfrac{C}{E}H(\epsilon_c)}, \tag{A4}$$

where

$$H(\epsilon) = \frac{1}{\epsilon} - \frac{1}{1-\epsilon} + \left(\frac{\tau}{\tau+1}\right)^2 \left(\frac{1}{2} - \epsilon\right) - \frac{2\tau+1}{(\tau+1)^2} \log \frac{1-\epsilon}{\epsilon}. \quad \text{(A5)}$$

The normalization integral in Eq. (A4) extends only to $\epsilon = \frac{1}{2}$ because the outgoing electron of higher energy is, by definition, the primary electron. Note that $H(\frac{1}{2}) = 0$, and that the probability, per unit path length, of an inelastic scattering with fractional energy transfer $\epsilon > \epsilon_c$ is

$$\mu_c(E) = NZ \int_{\epsilon_c}^{1/2} \frac{d\sigma}{d\epsilon}\, d\epsilon = \frac{NZC}{E} H(\epsilon_c). \quad \text{(A6)}$$

2. *Stopping Power for Electrons and Positrons*

Next we consider the mean energy loss by ionization per unit path length (stopping power) resulting from collisions with energy transfers $\epsilon < \epsilon_c$,

$$-\left(\frac{dE}{ds}\right)_{\epsilon_c} = NZ \int_0^{\epsilon_c} \epsilon \frac{d\sigma}{d\epsilon}\, d\epsilon. \quad \text{(A7)}$$

The integral in Eq. (A7) must be evaluated separately for the intervals $0 \leqslant \epsilon \leqslant \epsilon'$ and $\epsilon' \leqslant \epsilon \leqslant \epsilon_c$ ($\epsilon' \ll \epsilon_c$). In the first interval the Møller cross section (for scattering by free electrons) does not apply, and the binding of the atomic electrons must be taken into account through the Bethe theory of stopping power, which predicts that for small ϵ'

$$\int_0^{\epsilon'} \epsilon \frac{d\sigma}{d\epsilon}\, d\epsilon = \frac{C}{E}\left\{\log\left(\frac{2E^2\epsilon'(\tau+2)}{I^2}\right) - \beta^2\right\}. \quad \text{(A8)}$$

The quantity I is the so-called mean ionization potential which can in principle be determined from atomic theory but in practice is obtained from experimental stopping power data. We have used the values $I = 163$ ev for aluminum, 305 ev for copper, 797 ev for gold, and 802 ev for lead.

In the second interval, the integral over the Møller cross section can be carried out. When the result is combined with Eq. (A8), the parameter ϵ' drops out, and one finds that

$$-\left(\frac{dE}{ds}\right)_{\epsilon_c} = NZC\left\{\log\frac{E^2(\tau+2)}{2I^2} + f^-(\tau, \epsilon_c) - \delta\right\}, \quad \text{(A9)}$$

where

$$f^-(\tau, \epsilon_c) = -1 - \beta^2 + \left(\frac{\tau}{\tau+1}\right)^2 \frac{\epsilon_c^2}{2} + \frac{2\tau+1}{(\tau+1)^2} \log(1-\epsilon_c) \quad \text{(A10)}$$
$$+ \log[4\epsilon_c(1-\epsilon_c)] + \frac{1}{1-\epsilon_c}.$$

The parameter δ which has been inserted into Eq. (A9) represents the density effect, i.e., the reduction of the mean energy loss caused by the polarization of the medium. We have used values for δ presented by Nelms (1958), which were in turn derived from calculations of Sternheimer (1952, 1953).

For positrons, the Bhabha cross section for scattering by electrons must be used, and the upper limit of the fractional energy loss ϵ is one rather than one half. The stopping power for positrons (for $\epsilon_c = 1$) is obtained from Eq. (A9) with $f^-(\tau, \epsilon_c)$ replaced by

$$f^+(\tau, 1) = 2 \log 2 - \frac{\beta^2}{12}\left\{23 + \frac{14}{\tau + 2} + \frac{10}{(\tau + 2)^2} + \frac{4}{(\tau + 2)^3}\right\}. \quad \text{(A11)}$$

3. *Stopping Power for Protons*

We have used the tabulations of Sternheimer (1959) who computed the stopping power for protons from the expression

$$-\frac{dE}{ds} = NZC\left\{\log\left[\frac{2mv^2W_{\max}}{I^2(1-\beta^2)}\right] - 2\beta^2 - U - \delta\right\}, \quad \text{(A12)}$$

where

$$W_{\max} = \frac{\tau(\tau + 2)\, Mc^2}{\frac{M}{2m} + \frac{m}{2M} + \tau + 1} \quad \text{(A13)}$$

is the largest possible energy transfer in a collision between a proton and an atomic electron. U represents the so-called shell corrections taking into account the binding of the atomic electrons, and δ is again the density correction. Sternheimer's tabulated values were obtained with different values of the mean ionization potential I than those adopted in the present work, so that interpolation had to be used. Following a suggestion by Sternheimer (1960b) the interpolation was performed on the quantity $dE/ds\ A/Z$ which in very good approximation can be considered a function of $\log I$ only.

The mean pathlength traveled by the proton in the course of slowing down from energy E_0 to E is

$$\langle s \rangle_{\text{av}} = \int_E^{E_0} \frac{dE}{\left|\frac{dE}{ds}\right|}. \quad \text{(A14)}$$

The pathlength straggling has also been evaluated by Sternheimer (1960a) according to a theory of Bohr, from the expression

$$\langle s^2 \rangle_{\text{av}} - \langle s \rangle_{\text{av}}^2 = 4\pi e^4 N \int_E^{E_0} \frac{(1-\beta^2)^{-1}\,(1 - \frac{1}{2}\beta^2)\, K\, dE}{1 + \frac{2m}{M}(1-\beta^2)^{-1/2}\left|\frac{dE}{ds}\right|^3}, \quad \text{(A15)}$$

with the parameter K taking into account the binding of atomic electrons. Sternheimer has tabulated the percentage pathlength straggling

$$p_s = 100 \sqrt{\langle s^2 \rangle_{\mathrm{av}} - \langle s \rangle_{\mathrm{av}}^2} / \langle s \rangle_{\mathrm{av}} . \tag{A16}$$

Again interpolation was necessary. Following his suggestion (private communication) this was done assuming that p_s is a function of $\log I$ only.

4. *Distribution of Energy Losses*

If a particle with initial energy E_0 travels a pathlength s it will suffer an energy loss by ionization, ΔE, whose distribution has been derived by Landau (1944) for the case that $\Delta E \ll E_0$. His result can be expressed as

$$W_I(\Delta E)\, d(\Delta E) = W_L(\lambda)\, d\lambda , \tag{A17}$$

where

$$\lambda = \frac{\Delta E - \overline{\Delta E}}{NZCs} + \log \left(\frac{E_0}{NZC_s} \right) - 1.116 , \tag{A18}$$

$\overline{\Delta E}$ is the mean energy loss, and

$$W_L(\lambda) = \frac{1}{2\pi i} \int_{-i\infty+c}^{i\infty+c} \exp (u \log u + \lambda u)\, du \tag{A19}$$

is a universal function that has been evaluated by Landau and tabulated very completely by Börsch-Supan (1961).

Blunck and Leisegang (1950) have refined Landau's theory by considering in more detail the binding of the atomic electrons to which the particle transfers its energy. This results in a broadening of the energy loss distribution which is changed from $W_I(\Delta E)$ to

$$W_I^*(\Delta E) = \frac{1}{NZCsb\sqrt{\pi}} \int_{-\infty}^{\infty} W_I(\Delta E - u) \exp \left(- \frac{u^2}{NZCsb} \right) du , \tag{A20}$$

where the broadening parameter b can be expressed (Blunck and Westphal 1951) as

$$b = \sqrt{q \overline{\Delta E}}\, \frac{Z^{2/3}}{NZCs} , \tag{A21}$$

with $q \sim 20$ ev. A more detailed and complicated theory of the energy loss distribution has been developed by Symon and described by Rossi (1952).

B. Angular Deflections

1. *Evaluation of the Parameters in Molière's Theory*

Molière (1948) has given the following prescription for the evaluation of the parameters χ_c and B that enter into his distribution (Eq. 14 of the text) when energy loss is treated in the continuous-slowing-down approximation. It involves the computation of intermediate parameters χ_c', χ_a^2 and $\overline{\chi_a^2}$, according to the following prescription.

$$\chi_c'^2 = \frac{4\pi NZ^2}{p^2v^2}, \tag{A22}$$

$$\chi_c^2 = \int_0^s \chi_c'^2[s'(E)]\, ds' = \int_E^{E_0} \chi_c'^2(E') \left| \frac{dE}{ds} \right|^{-1} dE', \tag{A23}$$

$$\chi_a^2 = aZ^{2/3}\left[1.13 + 3.76\left(\frac{Z}{137\beta}\right)^2\right], \tag{A24}$$

[with $a = 6.8 \times 10^{-5}$ for electrons, $6.8 \times 10^{-5}\,(m/M)^2$ for protons] and

$$\log \overline{\chi_a^2} = \frac{1}{\chi_c^2} \int_E^{E_0} \chi_c'^2(E') \log \chi_a^2(E') \left| \frac{dE}{ds} \right|^{-1} dE'. \tag{A25}$$

The parameter B is obtained by solving the transcendental equation

$$B - \log B = \log \frac{\chi_c^2}{1.167\overline{\chi_a^2}}. \tag{A26}$$

The Molière theory takes into account only elastic collisions against the Coulomb field of atomic nuclei, but disregards inelastic collisions with atomic electrons. The latter have been considered by Fano (1954) who obtained corrections to Molière's theory. He finds that if the multiply-scattered particles are electrons, one must replace Z^2 by $Z(Z + 1)$ in Eq. (A22), and that one must add a term

$$B' = (Z + 1)^{-1}\left\{\log\left[0.160Z^{2/3}\left(1 + 3.33\left(\frac{Z}{137\beta}\right)^2\right)\right] - c_F\right\} \tag{A27}$$

on the right-hand side of Eq. (A26). For protons, one should leave Z^2 unchanged, but add to the right-hand side of Eq. (A26) a term

$$B'' = Z^{-1}\left\{\log\left[11.30Z^{-4/3}\frac{\beta^2}{1-\beta^2}\right] - c_F - \frac{1}{2}\beta^2\right\}. \tag{A28}$$

Fano has estimated the constant c_F to be -3.6 for hydrogen, -4.6 for lithium, -5.0 for oxygen, and -6.3 for lead. By interpolation we have

obtained values for other elements, e.g., -5.2 for aluminum and -6.2 for gold. The Fano correction was derived without taking into account the energy loss of the multiply-scattered particle. Little error will be incurred by evaluating it with a value of β corresponding to an energy intermediate between E_0 and E.

2. *Evaluation of the Goudsmit-Saunderson Theory*

This section makes use of various procedures developed by Spencer (1955, 1959) that facilitate the numerical evaluation of the Goudsmit-Saunderson angular multiple-scattering distribution

$$A_{Gs}(\omega) = \sum_{l=0}^{\infty} \left(l + \frac{1}{2}\right) \exp\left\{-\int_0^s G_l(s')\, ds'\right\} P_l(\cos\omega)\,. \tag{A29}$$

This Legendre series converges rather slowly, and the essential trick is to derive recursion relations with which a large number of the expansion coefficients can be computed accurately and easily.

a. Single-scattering cross section. The initial approximation is the Rutherford cross section for scattering of a charged particle by a nucleus of charge Ze,

$$\sigma_R = \frac{Z^2e^4}{p^2v^2(1-\cos\theta)^2}\,. \tag{A30}$$

The screening of the nuclear charge by orbital electrons can be taken into account approximately in various ways. We shall replace $(1-\cos\theta)^2$ by $(1-\cos\theta+2\eta)^2$, where η is a screening parameter that can be obtained from the theory of Molière as

$$\eta = \frac{1}{4}\chi_a^2\,, \tag{A31}$$

with χ_a^2 given by Eq. (A24). An improved formula for η has been given by Nigam *et al.* (1959) but not used in the present calculation. As can be seen from Eq. (A24), η is a very small quantity.

An improvement over the Rutherford cross section is provided by the Mott cross section σ_M which pertains to the scattering by an unscreened nuclear charge and is obtained through the exact solution of the Dirac equation (Mott, 1929). The cross section is obtained as a rather slowly converging Legendre series in the deflection angle, and must be evaluated numerically. Following earlier calculations by Bartlett and Watson (1940), Doggett and Spencer (1956), and Sherman (1956) have made systematic tabulations. Instead of interpolating in

these tables, we have used a FORTRAN computer program for the IBM 704 written by Dr. J. Coyne of the National Bureau of Standards. Typical ratios of the Mott to the Rutherford cross section for electrons and positrons, obtained with this program, are shown in Table XXI.

TABLE XXI

RATIO OF MOTT TO RUTHERFORD SCATTERING CROSS SECTION AT 0.5 MEV.

	Aluminum		Gold	
θ	Electrons	Positrons	Electrons	Positrons
0°	1.000	1.000	1.000	1.000
15°	1.019	0.961	1.083	0.919
30°	1.006	0.907	1.265	0.836
45°	0.962	0.839	1.508	0.757
60°	0.891	0.760	1.726	0.679
75°	0.862	0.732	1.851	0.605
90°	0.694	0.585	1.846	0.537
120°	0.481	0.419	1.472	0.421
150°	0.320	0.301	0.929	0.347
180°	0.260	0.259	0.678	0.320

Small deflections are particularly numerous and make an important contribution to the multiple-scattering angular distribution so that it is advantageous to take into account the analytical result that for small θ

$$\frac{\sigma_M}{\sigma_R} \sim 1 + \frac{\pi}{\sqrt{2}} \frac{Z\beta}{137} \cos\gamma \, (1 - \cos\theta)^{1/2} , \tag{A32}$$

where

$$\cos\gamma = Re \left\{ \frac{\Gamma\left(\frac{1}{2} - i\frac{Z}{137\beta}\right) \Gamma\left(1 + i\frac{Z}{137\beta}\right)}{\Gamma\left(\frac{1}{2} + i\frac{Z}{137\beta}\right) \Gamma\left(1 - i\frac{Z}{137\beta}\right)} \right\} . \tag{A33}$$

On combining the Rutherford cross section, the screening correction, the analytical form of σ_M/σ_R at small angles, and tabulated values of the Mott cross section, we adopt the following form for the single scattering cross section.

$$\sigma(\theta) = \frac{Z^2 e^4}{p^2 v^2 (1 - \cos\theta + 2\eta)^2} \times \left\{ 1 + \frac{\pi}{\sqrt{2}} \frac{Z\beta}{137} \cos\gamma (1 - \cos\theta + 2\eta)^{1/2} + h(\theta) \right\} , \tag{A34}$$

where the function

$$h(\theta) = \frac{\sigma_M}{\sigma_R} - 1 - \frac{\pi}{\sqrt{2}} \frac{Z\beta}{137} \cos \gamma (1 - \cos \theta + 2\eta)^{1/2} \tag{A35}$$

must be evaluated numerically.

Recently, Brown *et al.* (1961) have announced a numerical solution of the Dirac equation for scattering by a screened Coulomb potential. Their results will yield a cross section more accurate than Eq. (A34). Finally, we note that in Eq. (A34) Z^2 should be replaced by $Z(Z + 1)$ to take into account inelastic scattering. A further small correction has been suggested by Spencer, involving multiplication of the cross section by a factor $1 + B'/\log 4\eta$, with B' given by Eq. (A27).

The preceding formulation applies only to electrons and positrons but not to protons. For fast protons one must consider not only spin and relativistic effects, but also the influence of nuclear interactions, and the modification of Coulomb scattering by the finite size of the nucleus.

b. Expansion coefficients. The cross section $\sigma(\theta)$ enters into the Goudsmit-Saunderson distribution in the form of coefficients

$$G_l = 2\pi N \int_0^\pi \sigma(\theta) \{1 - P_l(\cos \theta)\} \sin \theta \, d\theta \, . \tag{A36}$$

For angular multiple-scattering distributions that are concentrated in the forward direction, a rather large number of G_l's may have to be evaluated. For example, in the example described in Table XXIV, the angular distribution multiplied by the solid-angle factor $\sin \omega$ peaks at 9.5° and as many as sixty terms in the Legendre expansion (A29) were used. To be accurate one should carry the integration in Eq. (A36) out analytically, particularly for large l. This can be done if the numerical part of the cross section, $h(\theta)$, is approximated by a polynomial, as follows:

$$h(\theta) = \sum_{j=1}^{J} h_j (1 - \cos \theta + 2\eta)^{j/2} \, . \tag{A37}$$

This representation has been found to be accurate to within 1% or better, with $J = 5$. Combining Eqs. (A34, A36, and A37), one finds that G_l can be expressed as a linear combination of integrals of the form

$$p(m, l) = \int_{-1}^{1} (1 - x + 2\eta)^m \{1 - P_l(x)\} \, dx \tag{A38}$$

for $m = -2, -3/2, -1, \ldots$, and for $l = 1, 2, 3, \ldots$. These integrals

can be evaluated by simple recursion relations that can be derived from the properties of Legendre polynomials. We shall merely state them briefly, referring the reader to Spencer (1955) for an explanation of the methods by which they are derived.

The first basic recursion, which allows one to go from m to $m + 1$, is

$$p(m+1, l) = (1 + 2\eta)\, p(m, l) + p(m, 1) - \frac{l+1}{2l+1}\, p(m, l+1) - \frac{l}{2l+1}\, p(m, l-1)\,. \tag{A39}$$

To start it, one needs to know $p(-2, l)$ and $p(-3/2, l)$ which can in turn be obtained from the following recursion relations:

$$\left.\begin{aligned} p(-2, 1) &= \log\left(1 + \frac{1}{\eta}\right) - (1+\eta)^{-1} \\ lp(-2, l+1) &= (2l+1)(1+2\eta)\, p(-2, l) \\ &\quad - (l+1)\, p(-2, l-1) - (2l+1)(1+\eta)^{-1}\,, \qquad l \geqslant 1 \end{aligned}\right\} \tag{A40}$$

and

$$\left.\begin{aligned} p(-\tfrac{3}{2}, 1) &= 2(2\tilde{\eta})^{3/2}(1+\tilde{\eta})^{-1} \\ p(-\tfrac{3}{2}, l+1) &= \tilde{\eta}\, p(-\tfrac{3}{2}, l) + p(-\tfrac{3}{2}, 1)\,, \qquad l \geqslant 1 \end{aligned}\right\}, \tag{A41}$$

where

$$\tilde{\eta} = 1 - 2\eta\{\sqrt{1 + 1/\eta} - 1\}\,. \tag{A42}$$

c. Energy dependence. The remaining task is to evaluate the integral

$$\int_0^s G_l(s')\, ds' \tag{A43}$$

in the continuous-slowing-down approximation. It is convenient to change variables from s to

$$t = \frac{r_0 - s}{r_0} \tag{A44}$$

where r_0 is the mean residual range, and make a corresponding change from $G_l(s)$ to $G_l^*(t)$. Spencer has shown that one can very accurately represent $G_l^*(t)$ by the expressions

$$G_1^*(t) = \frac{c_1}{t(t + c_2)} \tag{A45}$$

and

$$G_l^*(t) = G_1^*(t)\frac{G_l^*(1)}{G_1^*(1)}, \tag{A46}$$

where the two parameters c_1 and c_2 are obtained from a knowledge of $G_1^*(1)$ and $G_1^*(t)$. With this representation, one finds that

$$\begin{aligned}\int_0^s G_l(s')\,ds' &= r_0\int_i^1 G_l^*(t')\,dt' \\ &= r_0 c_1\frac{G_l^*(1)}{G_1^*(1)}\log\left\{\frac{t+c_2}{t(1+c_2)}\right\}.\end{aligned} \tag{A47}$$

Tables XXII and XXIII contain examples of Goudsmit-Saunderson distributions for electrons and positrons, for progressively longer

TABLE XXII

ANGULAR DISTRIBUTION OF MULTIPLY-SCATTERED ELECTRONS.[a]

E/E_0	$2^{-1/32}$	$2^{-1/16}$	$2^{-1/8}$	$2^{-1/4}$	$2^{-1/2}$	2^{-1}	2^{-2}
E (Mev)	0.489	0.479	0.459	0.420	0.354	0.250	0.125
$r(E)/r(E_0)$	0.970	0.942	0.886	0.784	0.611	0.363	0.120
ω	Angular distribution.						
0°	2.86(1)	1.25(1)	5.60	2.62	1.29	7.16(−1)	5.20(−1)
15°	9.43	7.67	4.55	2.40	1.25	7.08(−1)	5.19(−1)
30°	9.65(−1)	2.16	2.52	1.86	1.13	6.85(−1)	5.17(−1)
45°	1.35(−1)	4.45(−1)	1.03	1.23	9.52(−1)	6.48(−1)	5.14(−1)
60°	3.42(−2)	1.06(−1)	3.63(−1)	7.16(−1)	7.56(−1)	6.02(−1)	5.10(−1)
75°	1.24(−2)	3.45(−2)	1.26(−1)	3.78(−1)	5.69(−1)	5.49(−1)	5.05(−1)
90°	5.58(−3)	1.44(−2)	4.91(−2)	1.90(−1)	4.10(−1)	4.95(−1)	5.00(−1)
120°	1.63(−3)	3.91(−3)	1.16(−2)	4.97(−2)	1.97(−1)	3.96(−1)	4.90(−1)
150°	6.88(−4)	1.63(−3)	4.56(−3)	1.82(−2)	1.01 (−1)	3.28(−1)	4.83(−1)
180°	4.86(−4)	1.15(−3)	3.20(−3)	1.23(−2)	7.52(−2)	3.04(−1)	4.80(−1)

[a] For a pathlength in aluminum in which the energy is reduced from $E_0 = 0.5$ Mev to a value E, and the residual mean range from $r(E_0) = 0.2258$ gm/cm² to a value $r(E)$. Numbers in parentheses represent powers of ten.

pathlengths. Initially quite concentrated in the forward directions, the distributions rapidly become broader and practically isotropic when the particles have lost $\frac{3}{4}$ of their energy. Pertaining to the flux in an unbounded medium, they are more nearly isotropic, for long pathlengths, than the flux in the vicinity of the exit boundary of a foil, as can be verified through comparison with the results in Fig. 9. In Table XXIV,

TABLE XXIII

ANGULAR DISTRIBUTION OF MULTIPLY-SCATTERED POSITRONS.[a]

E/E_0	$2^{-1/32}$	$2^{-1/16}$	$2^{-1/8}$	$2^{-1/4}$	$2^{-1/2}$	2^{-1}	2^{-2}
E(Mev)	0.489	0.479	0.459	0.420	0.354	0.250	0.125
$r(E)/r(E_0)$	0.971	0.940	0.884	0.780	0.604	0.355	0.115
ω	Angular distribution.						
0°	3.08(1)	1.29(1)	5.85	2.74	1.36	7.48(−1)	5.29(−1)
15°	9.46	7.84	4.72	2.51	1.31	7.39(−1)	5.28(−1)
30°	8.64(−1)	2.13	2.55	1.92	1.17	7.11(−1)	5.25(−1)
45°	1.14(−1)	4.15(−1)	1.01	1.24	9.80(−1)	6.69(−1)	5.20(−1)
60°	2.82(−2)	9.44(−2)	3.38(−1)	7.02(−1)	7.66(−1)	6.15(−1)	5.14(−1)
75°	1.01(−2)	2.97(−2)	1.13(−1)	3.59(−1)	5.65(−1)	5.55(−1)	5.07(−1)
90°	4.52(−3)	1.22(−2)	4.23(−2)	1.73(−1)	3.97(−1)	4.93(−1)	5.00(−1)
120°	1.35(−3)	3.34(−3)	9.74(−3)	4.25(−2)	1.80(−1)	3.81(−1)	4.86(−1)
150°	6.11(−4)	1.47(−3)	3.95(−3)	1.51(−2)	8.70(−2)	3.06(−1)	4.75(−1)
180°	4.53(−4)	1.08(−3)	2.85(−3)	1.03(−2)	6.31(−2)	2.80(−1)	4.71(−1)

[a] For a pathlength in aluminum in which the energy is reduced from $E_0 = 0.5$ Mev to a value E, and the residual mean range from $r(E_0) = 0.2237$ gm/cm² to a value $r(E)$. Numbers in parentheses represent powers of ten.

TABLE XXIV

CONVERGENCE OF LEGENDRE-SUM FOR MULTIPLE-SCATTERING ANGULAR DISTRIBUTION.[a]

l_{max} \ ω	0°	15°	30°	60°
10	2.33965(1)	1.10424(1)	1.48240	−2.79748(−1)
20	2.84052(1)	9.40448	9.60956(−1)	4.53502(−2)
30	2.85867(1)	9.43132	9.64998(−1)	3.41642(−2)
40	2.85896(1)	9.43133	9.64688(−1)	3.41821(−2)
50	2.85896(1)	9.43132	9.64685(−1)	3.41835(−2)

l_{max} \ ω	90°	120°	150°	180°
10	−1.38927(−1)	−3.84342(−2)	6.81425(−2)	7.03439(−1)
20	1.03224(−2)	−4.21503(−3)	−5.33409(−3)	3.54991(−2)
30	5.51196(−3)	1.73052(−3)	5.58971(−4)	1.11688(−3)
40	5.57968(−3)	1.62751(−3)	6.87469(−4)	4.93515(−4)
50	5.57903(−3)	1.62765(−3)	6.87881(−4)	4.86467(−4)
60	5.57904(−3)	1.62765(−3)	6.87874(−4)	4.86400(−4)

[a] Pertains to the electron angular distribution given in the second column of Table XXII ($E/E_0 = 2^{-1/32}$). Numbers in parentheses represent powers of ten.

the convergence of the Legendre series for the angular distribution is illustrated, as a function of the number of terms, $l_{\max}$, retained in the expansion. Convergence is quite slow in the example, particularly at large angles. Thus at 150° the use of twenty terms would give a result which is ten times too large in absolute value and has the wrong sign, and almost sixty terms are required to provide convergence to six significant figures. The round-off error in the series summation has not yet been evaluated.

The cumulative form of the Goudsmit-Saunderson distribution, desirable for random sampling, can easily be obtained from the differential form, through replacing the Legendre polynomials $P_l(\cos\omega)$ in Eq. (A29) by

$$H_l(\cos\omega) = \int_{\cos\omega}^{1} P_l(x)\,dx\,, \tag{A49}$$

and use of the recursion relation

$$\left.\begin{aligned} H_0 &= 1 - \cos\omega \\ H_1 &= (1 - \cos^2\omega)/2 \\ (l+1)\,H_l &= (2l-1)\cos\omega H_{l-1} - (l-2)\,H_{l-2}\,, \qquad l \geqslant 2 \end{aligned}\right\}, \tag{A50}$$

References

Agu, B. N. C., Burdett, T., and Matsukawa, E. (1958a). *Proc. Phys. Soc. London.***71**, 201.
Agu, B. N. C., Burdett, T. A., and Matsukawa, E. (1958*b*). *Proc. Roy. Soc.* **72**, 727.
Archard, G. D. (1961). *J. Appl. Phys.* **32**, 1505.
Bartlett, J. H., and Watson, R. E. (1940). *Proc. Am. Acad. Arts Sci.* **74**, 54.
Berger, M. J. (1960). *Radiation Research* **12**, 422.
Bethe, H. A. (1935). *Proc. Roy. Soc.* **A150**, 129.
Bethe, H. A. (1953). *Phys. Rev.* **89**, 1256.
Bethe, H. A., Rose, M. E., and Smith, L. P. (1938). *Proc. Am. Phil. Soc.* **78**, 573.
Bichsel, H., and Uehling, E. A. (1960). *Phys. Rev.* **119**, 1670.
Birkhoff, R. D. (1958). *In* "Handbuch der Physik" (S. Flugge, ed.), Vol. 34, p. 53. Springer, Berlin.
Blanchard, C. H. (1951). *In* "Electron Physics" N.B.S. Circular 527, p. 9.
Blanchard, C. H., and Fano, U. (1951). *Phys. Rev.* **82**, 767.
Blunck, O., and Leisegang, S. (1950). *Z. Physik* **128**, 500.
Blunck, O., and Westphal, K. (1951). *Z. Physik* **130**, 641.
Börsch-Supan, W. (1961). *J. Research Natl. Bur. Standards* **65B**, 245.
Bothe, W. (1933). *In* "Handbuch der Physik" (H. Geiger ed.), Vol. 22, 2d ed., p. 1 Springer, Berlin.
Bothe, W. (1949). *Ann. Physik* **6**, 44.
Breitenberger, E. (1959). *Proc. Roy. Soc.* **250**, 514.
Brown, R. T., Lin, S. R., and Sherman, N. (1961). *Bull. Am. Phys. Soc.* **6**, 366.
Butcher, J. C., and Messel, H. (1960). *Nuclear Phys.* **20**, 15.

BUYS, W. L. (1960). *Z. Physik* **157**, 478.
CARLSON, B. G. (1955). Solution of the Transport Equation by S Approximations. Los Alamos Scientific Laboratory Report No. LA 1891.
DOGGETT, J. A., and Spencer, L. V. (1956). *Phys. Rev.* **103**, 1597.
EYGES, L. (1949). *Phys. Rev.* **76**, 264.
FANO, U. (1953). *Phys. Rev.* **92**, 328.
FANO, U. (1954). *Phys. Rev.* **93**, 117.
FLEISCHMANN, W. (1960). *Z. Naturforsch.* **15a**, 1090.
FRANK, H. (1959). *Z. Naturforsch.* **14a**, 247.
GOUDSMIT, S., and SAUNDERSON, J. L. (1940). *Phys. Rev.* **57**, 24.
HEBBARD, D. V., and Wilson, P. R. (1955). *Australian J. Phys.* **8**, 90.
KAHN, H. (1954). Application of Monte Carlo. U. S. AEC Report No. R-1237.
KANTER, H. (1957). *Ann. Physik* **20**, 144.
KOCH, H. W., and MOTZ, J. W. (1959). *Rev. Modern Phys.* **31**, 920.
LANDAU, L. (1944). *J. Phys. USSR* **8**, 201.
LEISS, J. E., PENNER, S., and ROBINSON, C. S. (1957). *Phys. Rev.* **107**, 1544.
LEWIS, H. W. (1950). *Phys. Rev.* **78**, 526.
LEWIS, H. W. (1952). *Phys. Rev.* **85**, 20.
MACCALLUM, C. (1960). *Bull. Am. Phys. Soc.* **5**, 379.
MATHER, R., and SEGRÈ, E. (1951). *Phys. Rev.* **84**, 191.
MCGINNIES, R. T. (1959). N.B.S. Circular 597.
MEISTER, H. (1958). *Z. Naturforsch.* 13a, 809.
MILLER, W. (1951). *Phys. Rev.* **82**, 452.
MOLIÈRE, G. (1947). *Z. Naturforsch.* **2a**, 133.
MOLIÈRE, G. (1948). *Z. Naturforsch.* **3a**, 78.
MOTT, N. F. (1929). *Proc. Roy. Soc.* **A124**, 475.
NELMS, A. T. (1958). N.B.S. Circular 577 (Supplement).
NIGAM, B. P., and MATHUR, V. S. (1961). *Phys. Rev.* **121**, 1577.
NIGAM, B. P., SUNDARESAN, M. K., and WU, T. (1959). *Phys. Rev.* **115**, 491.
ROESCH, W. C. (1954). Hanford Report No. HW 32121.
ROHRLICH, F., and CARLSON, B. C. (1954). *Phys. Rev.* **93**, 38.
ROSSI, B. (1952). "High Energy Particles." Prentice-Hall Englewood Cliffs, New Jersey.
SCHNEIDER, D. O., and CORMACK, D. V. (1959). *Radiation Research* **11**, 418.
SELIGER, H. H. (1952). *Phys. Rev.* **88**, 408.
SELIGER, H. H. (1955). *Phys. Rev.* **100**, 1029.
SHERMAN, N. (1956). *Phys. Rev.* **103**, 1601.
SIDEI, T., HIGASIMURA, T., and KINOSITA, K. (1957). *Mem. Fac. Eng. Kyoto Univ.* **19**, 22.
SNYDER, H. S., and SCOTT, (1949). *Phys. Rev.* **76**, 220.
SPENCER, L. V. (1955). *Phys. Rev.* **98**, 1507.
SPENCER, L. V. (1959). "Energy Dissipation by Fast Electrons." N. B. S. Monograph 1.
SPENCER, L. V., and Fano, U. (1954). *Phys. Rev.* **93**, 1172.
STERNHEIMER, R. M. (1952). *Phys. Rev.* **88**, 851.
STERNHEIMER, R. M. (1953). *Phys. Rev.* **91**, 256.
STERNHEIMER, R. M. (1959). *Phys. Rev.* **115**, 137.
STERNHEIMER, R. M. (1960a). *Phys. Rev.* **117**, 485.
STERNHEIMER, R. M. (1960b). *Phys. Rev.* **118**, 1045.
SUZOR, F., and CHARPAK, G. (1952). *J. phys. radium* **13**, 1.
TRUMP, J. G., and VAN de GRAAF, R. J. (1949). *Phys. Rev.* **75**, 44.
WANG, M. C., and GUTH, E. (1951). *Phys. Rev.* **84**, 1092.
WENTZEL, G. (1922). *Ann. Physik.* **69**, 335.

WEYMOUTH, J. W. (1951). *Phys. Rev.* **84**, 766.
WILLIAMS, E. J. (1939). *Proc. Roy. Soc.* **169**, 531.
WILSON, R. (1950). *Phys. Rev.* **79**, 204.
WILSON, R. (1951). *Phys. Rev.* **84**, 100.
YANG, C. N. (1951). *Phys. Rev.* **84**, 599.